RESEARCH ARTICLE

WILEY

Spontaneous synchronous network activity in the neonatal development of mPFC in mice

Johny Pires [iD] | Rosalie Nelissen | Huibert D. Mansvelder [iD] | Rhiannon M. Meredith [iD]

Department of Integrative Neurophysiology, Center for Neurogenomics & Cognitive Research, Faculty of Science, Neuroscience Campus Amsterdam, VU University Amsterdam, Amsterdam, the Netherlands

Correspondence
Johny Pires, Faculty of Science, Department of Integrative Neurophysiology, Center for Neurogenomics & Cognitive Research, Neuroscience, VU University Amsterdam, Campus Amsterdam, H226 VU Amsterdam, De Boelelaan 1085, 1081 HV, Amsterdam, The Netherlands.
Email: pires.johny@gmail.com

Funding information
Stichting voor de Technische Wetenschappen, Grant/Award Number: VIDI #917.10.372; EU MSCA-ITN CognitionNet, Grant/Award Number: FP7-PEOPLE-2013-ITN 607508

Abstract

Spontaneous Synchronous Network Activity (SSA) is a hallmark of neurodevelopment found in numerous central nervous system structures, including neocortex. SSA occurs during restricted developmental time-windows, commonly referred to as critical periods in sensory neocortex. Although part of the neocortex, the critical period for SSA in the medial prefrontal cortex (mPFC) and the underlying mechanisms for generation and propagation are unknown. Using Ca^{2+} imaging and whole-cell patch-clamp in an acute mPFC slice mouse model, the development of spontaneous activity and SSA was investigated at cellular and network levels during the two first postnatal weeks. The data revealed that developing mPFC neuronal networks are spontaneously active and exhibit SSA in the first two postnatal weeks, with peak synchronous activity at postnatal days (P)8–9. Networks remain active but are desynchronized by the end of this 2-week period. SSA was driven by excitatory ionotropic glutamatergic transmission with a small contribution of excitatory GABAergic transmission at early time points. The neurohormone oxytocin desynchronized SSA in the first postnatal week only without affecting concurrent spontaneous activity. By the end of the second postnatal week, inhibiting $GABA_A$ receptors restored SSA. These findings point to the emergence of $GABA_A$ receptor-mediated inhibition as a major factor in the termination of SSA in mouse mPFC.

KEYWORDS
brain development, calcium imaging, critical period, GABAergic system, mPFC, spontaneous synchronous network activity

1 | INTRODUCTION

In its immature state, the brain exhibits a variety of coherent, synchronous activity patterns reported in several areas of the nervous system across many species (Allene & Cossart, 2010). These areas include the retina, spinal cord, hindbrain, hippocampus, and many cortical regions (Moody & Bosma, 2005). Multiple in vivo and in vitro models demonstrate that cortical networks exhibit complex self-organized activity patterns even in the absence of sensory stimuli (Luczak & MacLean, 2012). Artificially disrupting these activity patterns elicits homeostatic mechanisms to maintain circuit output during neuronal network development, thus endorsing the necessity of Spontaneous Synchronous Network Activity (SSA) for proper network maturation (Blankenship & Feller, 2010; Stacy et al., 2005).

SSA dynamics are controlled by distinct molecular mechanisms that follow or trigger the maturation of physiological and morphological cellular properties (Khazipov & Luhmann, 2006; Luhmann & Khazipov, 2018; McCabe et al., 2006, 2007). This activity is derived from the intrinsic network architecture and cellular properties unique to early developmental stages. At prenatal stages, gap junctions, calcium channels, and cholinergic signaling underlie the earliest forms of synchrony in retinal and hippocampal circuits. However, at early postnatal stages, glutamatergic and GABAergic receptors mediate synchrony in neocortical and hippocampal circuits, respectively (Allene & Cossart, 2010; Picardo et al., 2011). Different networks mediate SSA through different developmentally restricted mechanisms, including early excitatory effects of gamma-aminobutyric acid (GABA) (Ben-Ari et al., 1989, 2012; Conhaim et al., 2011; Garaschuk et al., 2000) and high(er) connectivity through gap junctions (Blankenship & Feller, 2010; Dupont et al., 2006). Furthermore, a variety of cellular properties can increase neuronal excitability during the time period of SSA, including low-threshold calcium currents, high cell membrane resistance, and a different immature repertoire of ion channel subunit expression levels (Allene & Cossart, 2010; Barnett et al., 2014; Chamma et al., 2012; Corlew et al., 2004; Picken Bahrey & Moody, 2003).

The neocortex exhibits a variety of SSA patterns reflecting its complex developmental program (Luhmann et al., 2016). Relative to other neocortical regions, the medial prefrontal cortex (mPFC) is one of the brain areas with the longest maturational periods in humans (for review see (Schubert et al., 2015)) and is proposed to undergo some of the latest critical periods, not fully maturing until early adulthood (Thomas & Johnson, 2008). However, it is not confirmed whether mPFC development at the neuronal level is also protracted postnatally in rodents as in humans. An increasing body of research points toward the functional relevance of the mPFC from early on in postnatal life with involvement in functions such as social interaction and analyzing the emotions and intentions of others (Brumback et al., 2018; Gao et al., 2009; Gervain et al., 2008; Grossmann & Johnson, 2010). The functions and development of this area are especially relevant in autism spectrum disorders given their uneven profile of executive dysfunction and social deficits present even in high-functioning individuals (Gilbert et al., 2008; Pirone et al., 2018). Several studies point toward the impairment and dysfunction of deep layer neurons in the mPFC as a potential locus for autism pathology (Brumback et al., 2018). Yet, the trajectory of SSA and its underlying mechanisms during early postnatal development have not been fully explored in the rodent mPFC to-date.

In this study, multiphoton microscopy and whole-cell patch-clamp electrophysiology were used to infer the pattern of spontaneous activity and SSA within the developing mouse mPFC and to determine the underlying mechanisms. The data here presented shows that peak SSA occurs at the beginning of the second postnatal week and ceases by the end of this same week, marking a limited critical period for SSA in the developing mPFC. Gap junctions and oxytocin are capable of modulating subtle effects upon spontaneous activity and SSA during this early postnatal period. However, peak network synchrony is strongly mediated by ionotropic glutamatergic transmission. $GABA_A$ receptor-mediated signaling increases both spontaneous network excitation and SSA during the first postnatal week. In contrast, SSA can be restored by blockade of $GABA_A$ receptor-mediated inhibition at the end of the second postnatal week. Thus, excitatory and inhibitory signaling play dominant roles in the onset and cessation of SSA in the developing mPFC.

Highlights

- mPFC shows spontaneous and synchronous activity during the first two postnatal weeks
- Early postnatal activity in the mPFC is driven largely by glutamatergic transmission
- Oxytocin is able to desynchronize early network activity in the mPFC
- GABA blockade can partially restore SSA at the end of the second postnatal week

---

2 | MATERIALS AND METHODS

2.1 | Animal usage

All procedures involving animals were conducted in accordance with national Dutch regulations and were approved by an animal ethics committee (DEC) of the VU University Amsterdam. Male C57BL/6 mouse pups aged from postnatal day (P) 0 to P15, where P0 was taken as the day of birth, were used for slice preparation and data acquisition.

2.2 | Reagents

All reagents were purchased from Sigma-Aldrich except when indicated otherwise. The concentration of the drugs used for bath perfusion were: Tetrodotoxin (TTX):1 μM; Carbenoxolone (CBX): 100 μM; Glycyrrhizic acid (GZA): 100 μM; 6-cyano-7-nitroquinoxaline-2,3-dione (CNQX):10 μM; DL-2-Amino-5-phosphonopentanoic acid (DL-APV):50 μM; Gabazine (Tocris):10 μM; Oxytocin (OX): 1 μM.

2.3 | Preparation of coronal mPFC brain slices

Mouse pups were rapidly decapitated and their brains dissected out under ice-cold cutting solution containing (mM): 110 Choline chloride, 26 NaHCO3, 10 glucose, 11.6 sodium ascorbate, 3.1 sodium pyruvate, 2.5 KCl, 1.3 NaH2PO4 (Merck), 7 MgCl2, and 0.5 CaCl2 (Bureau et al., 2006); with osmolarity adjusted to 310 ± 5 Osm/L. Coronal slices of 300–350 μm (dependent on the age of the animal) were obtained using a Microm HM 650 V slicer (Thermo Fisher Scientific; frequency: 70 Hz, amplitude: 0.7 mm, speed: 0.07 mm/s). Slices were then allowed to recover for a minimum of 1 hr in a holding chamber containing slightly elevated magnesium artificial cerebral spinal fluid (aACSF) composed of (mM): 125 NaCl, 3 KCl, 1.2 NaH2PO4 (Merck),10 glucose, 26 NaHCO3, 2.5 MgCl2, and 1.6 CaCl2. The solution was continuously bubbled with carbogen gas (95% O2, 5% CO2).

2.4 | Bulk-loading acute brain slices

The bulk-loading of cells with Fura-2-AM was carried out as previously described in Dawitz et al (2011). Briefly, slices were transferred to a staining chamber containing 1 ml of aACSF (the same composition as previously mentioned aACSF, however, the magnesium concentration was 1.5 mM). This chamber was heated to 34°C and then 50 μg Fura-2-AM (Invitrogen) was diluted in 9 μl DMSO and 1 μl Pluronic acid (20% solution in DMSO; Invitrogen), vortexed for 5 min and pipetted directly on the slices. They were incubated for 20–40 min, depending on the age of the animal. After the incubation period, slices were placed into recording chambers that were previously coated with a poly(ethyleneimine)-solution, this coating discards the need for a metal harp as the slices stay slightly attached to the glass coverslip on the chamber. The chambers were then placed into a humidified interface constantly perfused with carbogen and left for a minimum of 1 hr before imaging.

2.5 | Two-photon calcium imaging

High-resolution videos were obtained using an Olympus microscope with a water immersion objective (20×; NA 0.95). One movie (per condition) was acquired on a Trimscope™ (LaVision Biotec) using a Ti-sapphire laser tuned to 820 nm. Images were captured using a Hamamatsu C9100 EM-CCD camera at 7.65 Hz for a total of 4,000 frames on an area of 450μmX525μm. During data acquisition, acute postnatal mouse brain slices were continuously perfused with oxygenated standard ACSF to approximately 37°C at 1 ml/min. After baseline recordings were obtained, drugs were washed into the bath for 10 min prior to reimaging under the new condition. At the end of each movie, a Z-stack $\pm$ 20 μm (in steps of 1 μm) of the focus plane was acquired for cell body detection. All data collection was done with ImSpector Software (LaVision BioTec).

2.6 | Analysis of imaging data

Custom-built scripts in Matlab (MathWorks, USA) were used to analyze the imaging data (full details in Hjorth et al., 2016). Briefly, neurons were detected using a Z-stack, for each condition, where an algorithm searched for local intensity maxima and a spherical region was analyzed around these centers creating individual regions of interest (ROI). These ROI were only added if the volume of the spherical region had a corresponding radius between 2 and 20 mm and a minimum area of 25 mm^2 intersection of the sphere and the imaging plane. For each cellular ROI, the correspondent intensity values of the pixels within were averaged per frame of the recording and plotted against the total time of recording to form a cell-specific activity trace. A running median of the relative trace was used to estimate a baseline, where frames with a > 10% drop in intensity, at least one standard deviation (SD) below the baseline and remained significantly below this baseline for a minimum of five frames (tested with a one-sided t test) were considered as a putative events. This procedure was repeated three times, excluding previously detected putative events and using ever so stricter two-sided t test comparing the new putative event frames against the filtered baseline. Results were manually inspected and corrected when necessary.

To detect synchronous network events (SSA) and to group neurons as being synchronous, first, the onset time of their events was summed on a frame-by-frame scheme and the activity vector resulting from this was smoothed by a Gaussian full width at half-maximum of five frames (500 ms).This activity vector will therefore represents a summary of the activity present. Second, a threshold was set as five times the standard deviation of 500 activity vectors that were created by randomly shuffling the inter-event intervals of the original activity vector. This threshold value consequently is calibrated per individual slice, dependent on both the number of active cells within the slice and their rates of activity. All events exceeding this threshold were considered as network events (reported as SSA in the Results). Cells that at least 40% of network events during the trace were then considered synchronous (SSA cells) (Hjorth et al., 2016). This will then categorize neurons into silent (no activity shown), active (at least one spontaneous event was detected) and SSA (which fulfill the criteria mentioned above). In the text, reported values for the percentages of active and synchronized cells are given to the nearest integer.

2.7 | Electrophysiological recordings and data analysis

The procedure for brain slice preparation was the same as for calcium imaging with the exception of dye-loading and slices were position into their recording chamber by a metal harp. The rate of perfusion, temperature, and running ACSF composition for baseline recording was kept as previously mentioned. All cells were pyramidal neurons recorded in layer 5 of the mPFC. These cells were viewed under infrared-differential interference contrast illumination and identified by their large triangular-shaped somata with a prominent dendrite and characteristic firing properties (Lee et al., 2014; Song & Moyer, 2018). For each brain slice, the boundaries of layer 5 was determined by observing the somata of these cells, which were typically located in a dense layer between 300 and 450 μm from the pial surface. At older ages Layer 2/3 could also be easily identified with similar characterizes but closer to the pial surface. Patch pipettes were pulled to a resistance of 3–5 MΩ and back-filled with high Cl- intracellular solution (pH 7.3, 290–295 mOsm) composed of (in mM): 70 K-Gluconate, 70 KCl, 10 HEPES, 4 Mg-ATP, 4 phosphocreatine, and 0.4 GTP. All recordings were done using a Multi-Clamp 700B amplifier (Molecular Devices, Palo Alto, CA, USA), low-pass-filtered at 3 kHz, sampled at 10 kHz, digitized using a Digidata 1440A (Molecular Devices, Palo Alto, CA, USA), and stored in a PC using Clampex 10.1 (Molecular Devices). After breakthrough, pyramidal cells were injected with several step pulses to estimate several parameters. For cells from younger animals (usually less than P6), the protocol started at −25 pA and increased in steps of 5 pA for a duration of 750 ms. For cell from older animals, the protocol started at −100 and increased in steps of 25 pA for a duration of 750 ms. For all voltage-clamp recordings, cells were held at −70 mV to isolate excitatory spontaneous synaptic activity, and recorded for 15 min for baseline levels (last 10 min used for analysis proposes), drugs were applied for 10 min and cells were then recorded another 10 min. For burst discharge measurements (Figures 5 and 6, Supporting Information Figure S1), layer 3 and 5 pyramidal neurons were identified in mPFC slices as before. Pipettes were filled with an intracellular solution containing (in mM): 125 Cs-gluconate, 5 CsCl, 4 NaCl, 10 HEPES, 0.2 EGTA, 2 K2-phosphocreatine, 2 Mg-ATP, 0.3 GTP, adjusted with KOH to pH 7.3 (±290 mOsm). Recordings of 5 min were made per cell and cells were clamped at −70 mV. Electrophysiological data were analyzed offline using Mini Analysis Program 6.0.7 (Synaptosoft, Decatur, GA, USA) for excitatory synaptic events and burst discharges and MATLAB (MathWorks, USA) for extracting and calculating basic cell properties.

2.8 | Statistics

Data are presented as mean ± *SEM*, except when non-normally distributed where median values are reported. Statistical significance was calculated using Kruskal–Wallis test, paired and unpaired *t* tests, Wilcoxon test, Mann–Whitney U test, Friedman test, and two-way ANOVA (GraphPad Prism; GraphPad Software, Inc., La Jolla, CA, USA). Nonparametric test statistics were used when normal distribution of analysis results could not be proven.

3 | RESULTS

3.1 | SSA peaks at the start of the second postnatal week in mouse mPFC

To map the critical period of SSA in the mPFC, acute coronal brain slices were imaged using the calcium-dependent indicator Fura-2 from birth (P0) to the end of the second postnatal week. The orientation of acute mPFC brain slices was chosen to preserve as much as possible the columnar structure of the mPFC by cutting parallel to the apical dendrites and studied activity in the mPFC without most of its connection to other brain areas. Per condition a 450 μm by 525 μm area was imaged for 4,000 frames at 7.65 Hz (131 ms exposure) with a 2-by-2 binning. A minimum of 20 cells on the focal plane was necessary for slice consideration. At the end of each condition a Z-stack using a step size of 1 μm at ±20 μm from the focal plane was done for later 3D reconstruction of the soma.

mPFC networks were composed of silent and spontaneously active cells, with a percentage of the active cells being synchronously active (Figure 1a–c). Spontaneous activity altered significantly during the first two postnatal weeks of development (Figure 1d,e, Table 1). The percentage of active cells within a network increased from 22 ± 4% (mean ± *SEM*) at P0–1 to its peak at P8–9 (35 ± 2.6%), before decreasing to its lowest level at the end of the second postnatal week (P14–15:11 ± 2%). Within the network, the proportion of cells whose activity was synchronous with each other (see Methods for definition) also changed significantly over developmental age (Figure 1d, discontinuous line). At both the start of the first postnatal week and end of the second postnatal week, very few cells were synchronously active (P0–1:4 ± 1.8%, P14–15:3 ± 1.5%). However, the proportion of synchronously active cells reached peak levels at P8–9 (20 ± 2% of total cells), coincident with peak levels of active cells within a network.

Of the cells that were active within a network, the frequency of their activity also changed significantly over the first two postnatal weeks (Figure 1e). Spontaneous activity was fairly constant around 0.01 to 0.015 Hz. During this same

time period, the frequency of synchronously active cells also altered significantly although in a distinct pattern to general spontaneous activity (Figure 1e). Synchronous network activity (SSA) was negligible at P0–1 (0.0009 ± 0.0004 Hz) but increased to reach a peak at the start of the second postnatal week (P8–9:0.01 ± 0.001 Hz), before declining to a near-absence at P14–15 (0.0007 ± 0.0003 Hz).

The amplitude and area under the curve (AUC) of calcium events in active cells (Supporting Information Figure S1a–c) was significantly affected by age with the P0–6 group being significantly higher (amplitude 0.104 ± 0.003, AUC 3.93 ± 0.50) than both P7–9 (amplitude 0.093 ± 0.004, AUC 1.75 ± 0.14) and P10–15 (amplitude 0.079 ± 0.005, AUC 1.78 ± 0.30). SSA cells showed a similar outline with both parameters being significantly affected by age and P0–6 (amplitude 0.114 ± 0.006, AUC 3.05 ± 0.34) showing significantly higher values in both parameters than P10–15 (amplitude 0.084 ± 0.006, AUC 1.63 ± 0.36) and higher AUC than P7–9 (amplitude 0.102 ± 0.005, AUC 1.41 ± 0.11).
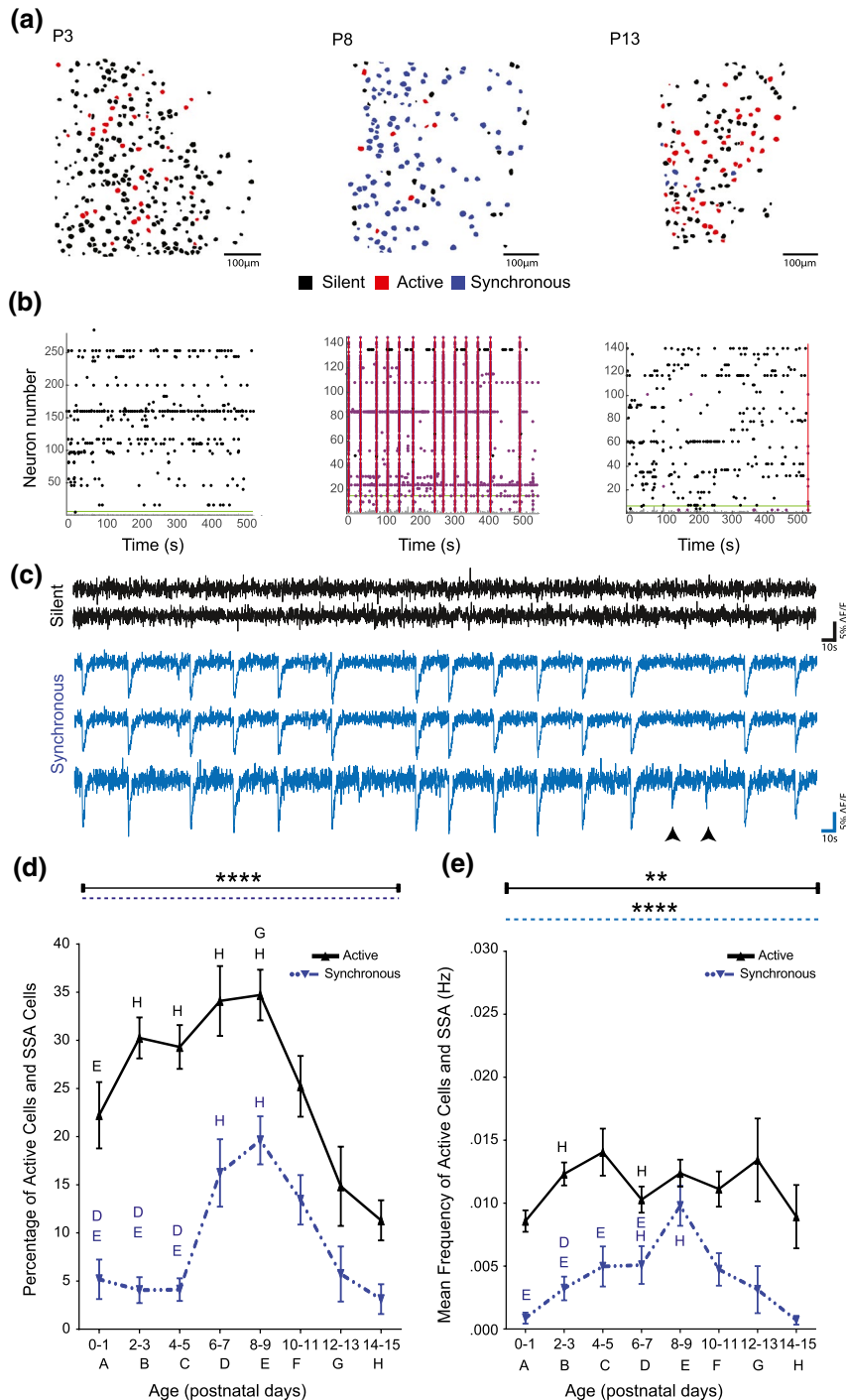
FIGURE 1 Peak network synchrony (SSA) in mPFC occurs at the beginning of the second postnatal week. (a) Semiautomatically detected contours of the cells (masks) present on the focal plane of the example time-lapse recordings at ages P3, P8, and P13. Black-filled contours indicate silent cells, red-filled indicate cells that were active but no activity was synchronous, and blue-filled indicate active cells that were synchronous in at least one network event. Scale bar, 100 μm. (b) Raster plots of the activity from the same slices whose masks are represented in (a). Each identified cell is represented in a single row and the beginning of a detected event is marked with a single dot. The green horizontal line represents the iterative threshold for the detection of SSA. Fuchsia colored dots indicate events classified as an SSA event. (c) Five representative traces taken from the P8 example slice during a typical recording. Two silent cells (black traces) and three synchronized cells (blue traces) are shown. Arrowheads indicate spontaneous activity in the cell that was outside of SSA. (d) Percentage of active and synchronized cells from P0 to P15 in the mPFC. Overall spontaneous activity changed significantly with postnatal age in terms of percentage of active cells (Kruskal–Wallis H (8) = 46.73, $p < .0001$) with a significant decrease toward latest time point (P14–15) (Pairwise comparisons with independent samples Kruskal–Wallis test P0–1 vs. P8–9, $p = .036$; P2–3 vs. P14–15, $p < .0001$; P4–5 vs. P14–15, $p < .0001$ P6–7 vs. P14–15, $p < .0001$; P8–9 vs. P12–13, $p = .013$ and vs. P14–15, $p < .0001$). Similarly the percentage of cells whose activity is synchronized in the network, varied significantly with postnatal age (Kruskal–Wallis H (8) = 49.29. $p < .0001$). SSA peaked at P6–9 from low values that decreased to near zero values by the end of the second postnatal week (Pairwise comparisons with independent samples Kruskal–Wallis test P0–1 vs. P6–7, $p = .035$ and vs. P8–9, $p < .0001$; P2–3 vs. P6–7, $p = .001$ and vs. P8–9, $p < .0001$; P4–5 vs. P6–7, $p = .039$ and vs. P8–9, $p < .0001$; P6–7 vs. P14–15, $p = .031$; P8–9 vs. P14–15, $p < .0001$). (e) Frequency of spontaneous activity and SSA from P0 to P15 in the mPFC. The frequency of spontaneously active cells, similarly to the percentage of active cells, was significantly affected by age (Kruskal–Wallis H (8) = 19.99, $p = .0056$). SSA frequency, on the contrary, showed a bell-shaped pattern demonstrating a significant effect of age (Kruskal–Wallis H (8) = 41.70, $p < .0001$). The activity rose during the first 7 days, peaking at P8–9, and decreasing to near zero values by P15 (Pairwise comparisons with independent samples Kruskal–Wallis test P0–1 vs. P8–9, $p < .0001$; P2–3 vs. P6–7, $p = .012$ and vs. P8–9, $p < .0001$; P4–5 vs. P8–9, $p < .0001$; P6–7 vs. P8–9, $p < .0001$ and vs. P14–15, $p = .045$; P8–9 vs. P14–15, $p < .0001$). Data were not normally distributed. Total number of slices per age group is: P0–1: $n = 34$. P2–3: $n = 64$. P4–5: $n = 55$. P6–7: $n = 48$. P8–9: $n = 80$. P10–11: $n = 54$. P11–12: $n = 13$. P14–15: $n = 25$ [Color figure can be viewed at wileyonlinelibrary.com]

Thus, the immature mPFC exhibits a developmentally regulated pattern of SSA that increased during the first postnatal week, peaked at the start of the second postnatal week and then virtually disappeared, although the network remained spontaneously active. These activity profiles indicate critical period for SSA in the mPFC during P0 to P15, since mPFC networks can remain spontaneously active after P14–15 but synchronous activity is no longer present.

3.2 | SSA is partially intrinsic to the immature mPFC

To determine whether the mPFC by itself can maintain or self-generate spontaneous and synchronous activity, network activity was measured in mPFC networks (P7–9) before and after isolation of the surrounding cortical tissue, utilizing a minislice preparation (Figure 2a). Following mPFC isolation,

TABLE 1 Percentages and frequency of spontaneously active and SSA in developing mPFC networks

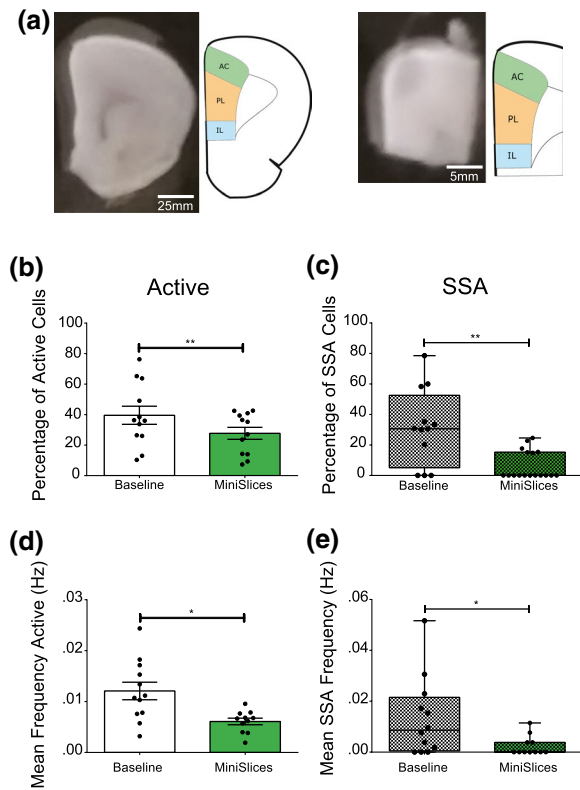| Age | Active | | SSA | | Number of slices |
---	Mean	SD	Mean	SD	
0–1	22.22%	±20.09	3.8%	±10.48	34
	0.008572 Hz	±0.004968	0.000866 Hz	±0.002575	
2–3	30.25%	±17.04	4.1%	±10.74	64
	0.012315 Hz	±0.007293	0.003224 Hz	±0.007515	
4–5	29.31%	±16.86	4.11%	±8.7	55
	0.014044 Hz	0.013869	0.004964 Hz	±0.011807	
6–7	34.1%	±25.14	16.22%	±24.28	48
	0.010278 Hz	±0.007186	0.005081 Hz	±0.010361	
8–9	34.71%	±25.53	19.61%	±22.32	80
	0.012378 Hz	±0.009628	0.009788 Hz	±0.014202	
10–11	25.23%	±23.19	13.44%	±18.89	54
	0.011117 Hz	±0.010296	0.004736 Hz	±0.009505	
12–13	14.85%	±14.84	5.73%	±10.32	13
	0.018736 Hz	±0.015305	0.003130 Hz	±0.006735	
14–15	11.3%	±10.43	3.12%	±7.74	25
	0.018487 Hz	±0.038216	0.000697 Hz	±0.001735	

FIGURE 2 Low level spontaneous activity and SSA persist in isolated mPFC. (a) Acute coronal slice from a P8 animal before and after the isolation of the mPFC. The cartoon (left) shows the mPFC with the anterior cingulate (AC), prelimbic (PL), infralimbic (IL) cortices, and forceps minor of the corpus callosum (FMI). The cartoon (right) displays the areas still present in the minislice after the isolation of the mPFC. (b) Significant decrease in the percentage of active cells following mPFC isolation (t (11) = 3.106, p = .01, two-tailed). (c) Significant reduction but persistence of synchronized cells after mPFC isolation (Mann–Whitney U = 36.50, p = .0014). (d) The frequency of active cells significantly decreased following mPFC isolation (t (10) = 3.57, p = .012). (e) Reduction but persistence of SSA in a subset of minislices (5/12) following mPFC isolation (Mann–Whitney U = 32.00, p = .0284). N = 12 for both baseline and minislices. *p < .05; **p < .01; ***p < .001; ****p < .0001 [Color figure can be viewed at wileyonlinelibrary.com]

the percentage of active cells within the network and their mean frequency of activity decreased significantly (Figure 2b, active cells: 40 ± 6.0% vs. 28 ± 4%, and Figure 2d, active cell frequency: 0.012 ± 0.002 vs. 0.0061 ± 0.0007). However, spontaneous activity persisted in all minislice preparations imaged. Similarly, the percentage of synchronized cells and their network frequency also decreased significantly following mPFC isolation (Figure 2c, synchronous cells: 31 ± 7% vs. 7 ± 2%; Figure 2e, SSA: 0.013 ± 0.0045 Hz vs. 0.0024 ± 0.0012 Hz). However, unlike spontaneous activity levels within the mPFC network, SSA disappeared in the vast majority of slices, with only a subset of slices (n = 5/12) maintaining a small percentage of synchronized cells firing simultaneously at a low frequency. Therefore, the mPFC can
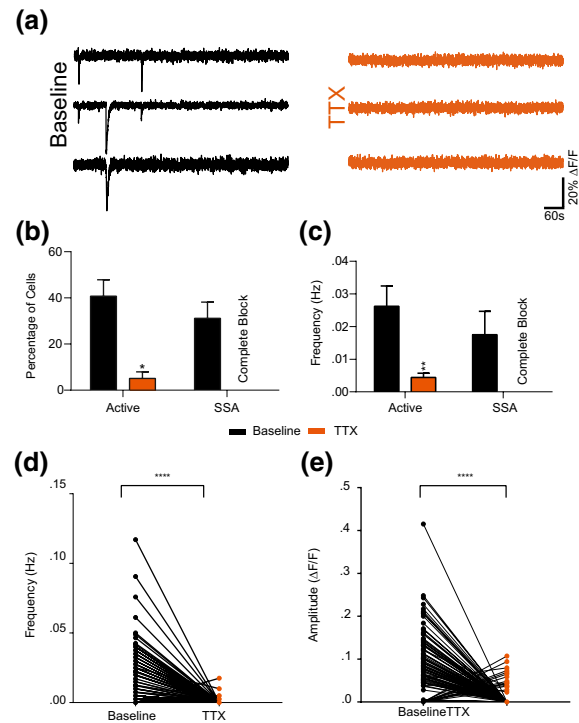

FIGURE 3 SSA is action potential-dependent in the developing mPFC. (a) Example traces from Ca^{2+} recordings at baseline (black) and after TTX incubation (orange). (b) TTX decreased both the percentage of active (paired t test, t (5) = 3.71, p = .0139) and synchronized cells within a network (paired t test, t (5) = 4.083, p = .0095). (c) Similarly, TTX application decreased the frequency of spontaneously active cells (paired t test, t (4) = 3.859, p = .0182) and led to a complete block of SSA (t (5) = 3.544, p = .0165). (d) A cell-to-cell comparison confirms a significant decrease of frequency of spontaneous events (paired t test, t (224) = 6.481, p < .0001). (e) Similarly, a paired comparison reveals a significant drop in signal amplitude after the application of TTX (paired t test, t (220) = 7.310, p < .0001). For all conditions n = 6. *p < .05; **p < .01; ***p < .001; ****p < .0001 P7–9, n = 6 [Color figure can be viewed at wileyonlinelibrary.com]

maintain spontaneous activity in isolation, and albeit at a reduced level and in a subset of cases, some persistent SSA remains.

3.3 | Spontaneous and synchronous activity in the mPFC depend on action potentials

Several studies show that cortical neuronal activity is accompanied by an intracellular calcium rise that is either caused by a depolarization in the membrane potential (Allene et al., 2008; Corlew et al., 2004; Yang et al., 2009) or by intracellular mechanisms that do not lead to a measurable electrical signal (Kandler & Katz, 1998; Yuste et al., 1992). To probe the mechanism used to initiate and maintain SSA, the sodium channel blocker tetrodotoxin (TTX) (Carter

& Bean, 2009) was applied to test if the spontaneous Ca^{2+} events were caused by action potential-dependent activity.

Addition of TTX (1 μM) significantly decreased both the percentage of active cells and their frequency (Figure 3a–c, baseline 41 ± 18% vs. TTX 5 ± 7%, frequency baseline 0.026 ± 0.015 Hz vs. TTX 0.0044 ± 0.0031). Furthermore, TTX induced a complete block of all synchronized activity within mPFC networks and no synchronized cells were present in any of the slices tested (Figure 3b,c, baseline 31 ± 17% vs. TTX complete block; frequency baseline 0.018 ± 0.017 Hz vs. TTX complete block). A cell-to-cell comparison of all imaged networks confirmed this significant decrease in both frequency (Figure 3d, paired t test, t (224) = 6.481, $p < .0001$) and amplitude of the signals (Figure 3e, paired t test, t (220) = 7.310, $p < .0001$). These results demonstrate a clear action potential-dependence of SSA in mPFC, which could be mediated throughout the network via electrical and/ or chemical synaptic transmission.

A small percentage of cells (14/225 ~ 6%) actually had their activity increased by the presence of TTX, and all but one were silent before the application of the drug.

A potential explanation would be disinhibition but this would need to be tested due to the fact that the GABAergic system might not yet assume an inhibitory role, also a recruitment or enhancement of apparently silent postsynaptic synapses could have contributed to this phenomena.

Another potential explanation would be an homeostatic adaptation to maintain an optimal level of neuronal activity as blockade of spontaneous network activity with TTX has been shown to an increase the frequency and amplitude of AMPA receptor-mediated mEPSCs in newborn rat hippocampus (Chowdhury & Hell, 2018; Lauri et al., 2003; Turrigiano & Nelson, 2004). In the retina, which shows several sequential mechanisms responsible for SSA, the blockade of one of this mechanisms makes the retina regresses to the previous wave-generating mechanism (Blankenship & Feller, 2010).

3.4 | Involvement of gap junctions in mPFC SSA

At very early stages of cortical development, chemical synapses are scarce but the neocortex already expresses gap junctions that are involved in various processes such as neurogenesis, cell migration, and synapse formation (Connors et al., 1983; Sutor & Hagerty, 2005). In newborn mice (P0–3), studies reported the involvement of gap junction in synchronous plateau assemblies (Allene et al., 2008; Dupont et al., 2006) and in older animals (P8–14), being involved in spreading waves of activity (Siegel et al., 2012). Therefore, to test the influence of gap junctions on early spontaneous and synchronous activity, slices from P0–3 mice were imaged under baseline conditions and either carbenoxolone (CBX,

100 μM) or its inactive (regarding gap junction blockade) analog, glycyrrhizic acid (GZA, 100 μM) (Bani-Yaghoub et al., 1999) were acutely applied.

The presence of CBX or GZA had no significant effect on either the percentage of active cells or their frequency (Figure 4 B and D). The presence of CBX, however, increased the percentage of synchronized cells (Figure 4c, synchronized baseline median = 0%, CBX = 4%) and their network frequency (Figure 4e, SSA frequency baseline median = 0 Hz, CBX = 0.002 Hz), although it is important to note that baseline SSA is at a low level at this immature stage of development (see confirmation in Figure 1e and example of a typical raster plot in Figure 4a). As a control, no significant changes were observed with application of glycyrrhizic acid for spontaneous activity or SSA in the mPFC (Figure 4b–e). Therefore, pharmacological blockade of gap junctions appeared to have a small facilitatory effect on SSA in the first few postnatal days of mPFC development, without an effect on general spontaneous activity.

3.5 | Maturing glutamatergic synaptic transmission underlies SSA in the developing mPFC

Excitatory synaptic transmission is a predominant feature of the first postnatal week of the development of rodent neocortex (Hestrin, 1992; Sutor & Hagerty, 2005). Neocortical forms of SSA has been shown to involve AMPA- and NMDA-type glutamate receptors (Garaschuk et al., 2000; McCabe et al., 2006) with NMDA receptor signaling appearing early on during network formation and regulating the synaptic recruitment of AMPARs (Allene & Cossart, 2010). To test the involvement of ionotropic glutamate receptors in spontaneous activity and SSA in the developing mPFC, neuronal activity at different postnatal days was imaged before and after incubation with a combination of CNQX and DL-APV (Figure 5a). The combination of CNQX and DL-APV decreased the percentage of active cells in ages older than P7 with the more pronounced effect on the P7–9 age group (Figure 5b, Percentage of Active: P7–9 baseline = 36±2% vs. CNQX + DL-APV = 13±0.2%, Mann–Whitney U = 806.5, $p < .0001$; P10–14 baseline = 20±2% vs. CNQX + DL-APV = 12±2%, Mann–Whitney U = 1,747, $p = .0277$). There was no significant effect on the frequency of spontaneous activity at any age measured (Figure 5c). However, blocking AMPA- and NMDA receptors significantly reduced the number of synchronous cells in all age groups measured, with the biggest reduction being seen in the P7–9 groups, similar to that observed for spontaneous activity (Figure 5d, Percentage of SSA cells: P0–6 baseline = 5±1% vs. CNQX + DL-APV = 3±1.0%, Mann–Whitney U = 5,439, $p = .0027$; P7–9 baseline = 20±2% vs. CNQX + DL-APV = 3±1%, Mann–Whitney U = 1,030, $p < .0001$; P10–15
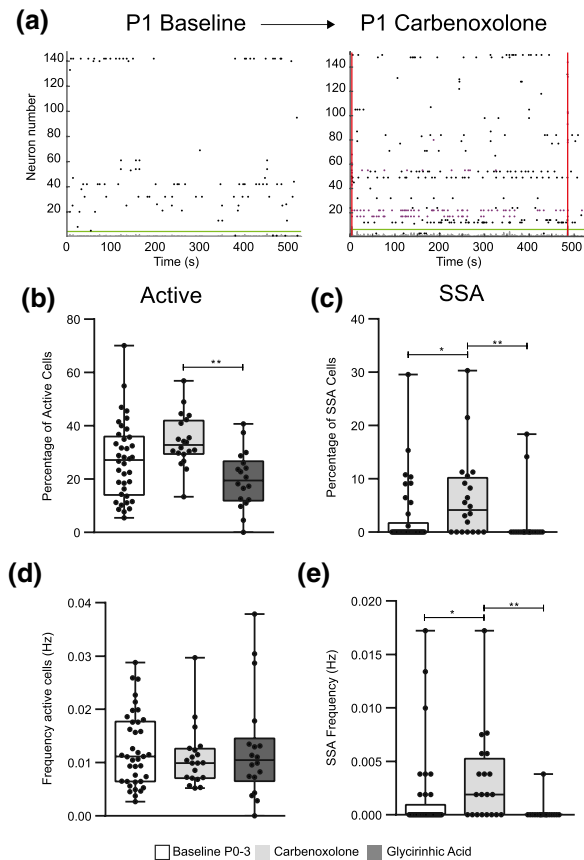
FIGURE 4 Influence of gap junctions on early SSA. All slices recorded were from animals from P0 to P3. (a) Example raster plots of a P1 slice before and after the incubation with gap junction blocker Carbenoxolone. (b) An ANOVA of the percentage of active yielded significant variation between the conditions, $F(2, 73) = 6.437$ $p = .0027$. A post hoc Tukey test showed that CBX and GZA differed significantly at $p < .01$. However, none of the drug condition significantly changed this when in comparison with the baseline (mean $\pm$ *SEM*: baseline 21.0 ± 2.35, CBX 34.4 ± 2.18, GZA 19.8 ± 10.70). (c) CBX increased the percentage of synchronized cells in a network (Kruskal–Wallis, H (3) = 11.64, $p = .003$; Dunn's multiple comparisons test Baseline vs. Carbenoxolone, mean rank difference = -14.28, $p < .05$). GZA showed no significant change relative to baseline but a significant difference when compared to CBX (Dunn's multiple comparisons test CBX vs. GZA, mean rank difference = 19.04, $p < .01$). (d) CBX or GZA application had no significant effect upon the frequency of spontaneously active cells. (e) CBX application increased the SSA frequency (Kruskal–Wallis, H (3) = 13.1, $p < .001$, Dunn's multiple comparisons Baseline vs. CBX, mean rank difference = -13.07, $p < .05$). GZA showed no significant change upon SSA frequency relative to baseline but significantly differed from CBX (Dunn's multiple comparisons CBX vs. GZA, mean rank difference = 19.98, $p < .01$). Baseline $n = 38$, CBX $n = 20$, GZA $n = 18$. *$p < .05$; **$p < .01$; ***$p < .001$; ****$p < .0001$ [Color figure can be viewed at wileyonlinelibrary.com]

baseline = $10\pm2\%$ vs. CNQX + DL-APV = $2\pm1\%$, Mann–Whitney U = 1,742, $p = .0046$). Similarly, SSA frequency significantly decreased by blocking ionotropic glutamatergic

transmission at all ages tested to very low levels (Figure 5e SSA frequency: P0–6 baseline = 0.0035 ± 0.0007 Hz vs. CNQX + DL-APV = 0.0007 ± 0.0003 Hz, Mann–Whitney U = 5,301, $p = .0008$; P7–9 baseline = 0.0088 ± 0.0013 Hz vs. CNQX + DL-APV = 0.0009 ± 0.0004 Hz, Mann–Whitney U = 1,039, $p < .0001$; P10–14 baseline = 0.0034 ± 0.0001 Hz vs. CNQX + DL-APV = 0.0007 ± 0.0003 Hz, Mann–Whitney U = 1,763, $p = .0066$).

To validate the developmental maturation of excitatory and glutamatergic activity underlying network activity in mPFC, spontaneous excitatory synaptic activity and network burst discharges from individual layer 5 pyramidal neurons were recorded. Burst discharges were prominent in 13/66 (~20%) neurons recorded (Figure 5f, see inset for enlarged trace) and exhibited a similar developmental profile to SSA measurements with peak frequency of burst discharges occurring at P7–9 (appearing in 12/31 neurons recorded) and a very low frequency or absence in P1–3 and P10–15 (Figures 1e and 5g). In-between burst discharge activity, spontaneous excitatory postsynaptic currents (sEPSCs) were measured from the same pyramidal neurons. sEPSC amplitude increased significantly during the first postnatal week, stabilizing during the second postnatal week (Figures 5h, P1–3 = 14.7 ± 1.2 pA, P4–6 = 20.3 ± 5.8 pA, P7–9 = 21.1 ± 6.2 pA, P10–15 = 20.9 ± 3.5 pA). sEPSC frequency also increased significantly with increasing developmental age (Figures 5i, P1–3 = 0.08 ± 0.03 Hz, P4–6 = 0.12 ± 0.02 Hz, P7–9 = 0.45 ± 0.12, P10–15:1.7 ± 0.37 Hz), with the highest levels and increased variability observed at P10–15, similar to the pattern of increasing spontaneous but non-synchronized activity recorded with calcium indicators (Figures 1e and 5i).

Thus, glutamatergic synaptic activity develops significantly during the first two postnatal weeks of mPFC development; ionotropic glutamate receptors mediate a significant proportion of spontaneous activity across the network and are the dominant mechanism underlying SSA in the developing mouse mPFC.

3.6 | Removal of GABAergic inhibition at the end of the second postnatal week restores SSA

Previous reports have demonstrated little or no role for GABAergic transmission, particularly GABA$_A$ receptors, underlying SSA in neocortical slices during the initial part of the first postnatal week, in contrast to generation of forms of SSA in the hippocampus (Allene et al., 2008; Allene & Cossart, 2010; Bonifazi et al., 2009; Garaschuk et al., 1998, 2000; Picardo et al., 2011). To determine the potential contribution of GABAergic transmission upon activity within the mPFC, we tested the effects of GABA$_A$ receptor-mediated inhibition by blocking both phasic and tonic elements of GABA$_A$ receptors (Figure 6a,b).
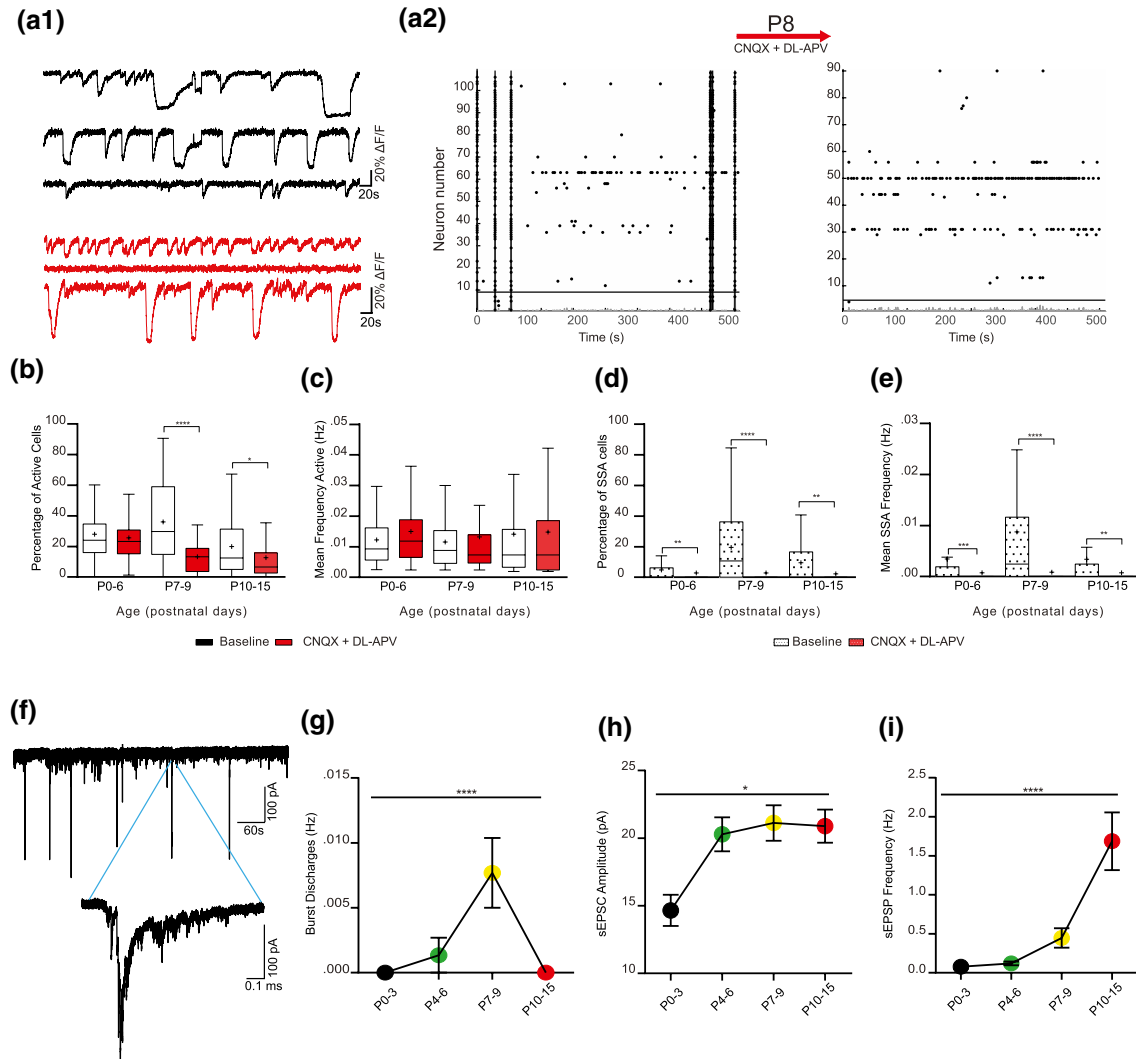
FIGURE 5 Glutamatergic synaptic transmission underlies SSA in the developing mPFC. (a1) Representative calcium fluorescence traces from a P8 slice at baseline (black) and after incubation with glutamatergic blockers (CNQX + DL-APV) (red). (a2) Raster plots from the slice whose traces are represented in (a1). (b) Blocking ionotropic glutamate transmission led to a decrease in the percentage of active cells in ages older than P7 (P7–9: Mann–Whitney U = 806.5, $p < .0001$; P10–15: Mann–Whitney U = 1747, $p = .0277$) but not in the P0–6 group. (c) The presence of CNQX + DL-APV did not alter the frequency of active cells in any age group. (d) CNQX and DL-APV significantly decrease the percentage of SSA cell in all age groups (P0–6: Mann–Whitney U = 5,439, $p = .0027$; P7–9: Mann–Whitney U = 1,030, $p < .0001$; P10–15: Mann–Whitney U = 1742, $p = .0046$) to values close or equal to zero. (e) Similar to the effect on the percentage of SSA cells, the presence of CNQX and DL-APV significantly decrease SSA frequency at all ages measured (P0–6: Mann–Whitney U = 5,301, $p = .0008$; P7–9: Mann–Whitney U = 1,039, $p < .0001$; P10–15: Mann–Whitney U = 1763, $p = .0066$) with values reaching a median of zero. (f) Trace example from a recording of sEPSC in a P8 layer 5 pyramidal neuron in the mPFC showing burst discharges. Insert shows an expanded view of one of the bursts showing the typical shape of a burst with a large depolarization followed by a plateau with multiple action potentials. (g) Frequency of Burst discharges detected while recording sEPSC. Age has an effect on the frequency of bursts (Kruskal–Wallis H = 29.12, $p < .0001$) with the P7–9 groups showing significantly higher values in comparison to other ages (Dunn's multiple comparisons test: P1–3 vs. P7–9 *, P4–6 vs. P7–9 ***, P7–9 vs. P10–15 *). (h) Maturation of Layer 5 PC EPSC amplitude during the first and second postnatal week displaying an increase over time (Kruskal–Wallis H (4) = 9.110, $p = .0279$) with the first postnatal day presenting significantly lower values when compared to the end time points (Dunn's multiple comparisons test: P1–3 vs. P7–9 *, P1–3 vs. P10–15 *). (i) Layer 5 PC EPSC frequency increases over the time period measured (Kruskal–Wallis H (4) = 25.85, $p < .0001$) with frequency at the end of the second postnatal week being significantly higher than the values on the first week (Dunn's multiple comparisons test: P1–3 vs. P10–15 ***, P4–6 vs. P10–15 ****). *$p < .05$; **$p < .01$; ***$p < .001$; ****$p < .0001$. *For calcium imaging (B-E) n = number of slices: P0–6 baseline n = 160, CNQX + DL-APV = 83; P7–9 baseline n = 112, CNQX + DL-APV = 34; P10–15 baseline n = 92, CNQX + DL-APV = 49. For patch-clamp (F-H) n = number of cells: P1–3 baseline n = 6; P4–6 baseline n = 21; P7–9 baseline n = 22; P10–15 baseline n = 8* [Color figure can be viewed at wileyonlinelibrary.com]
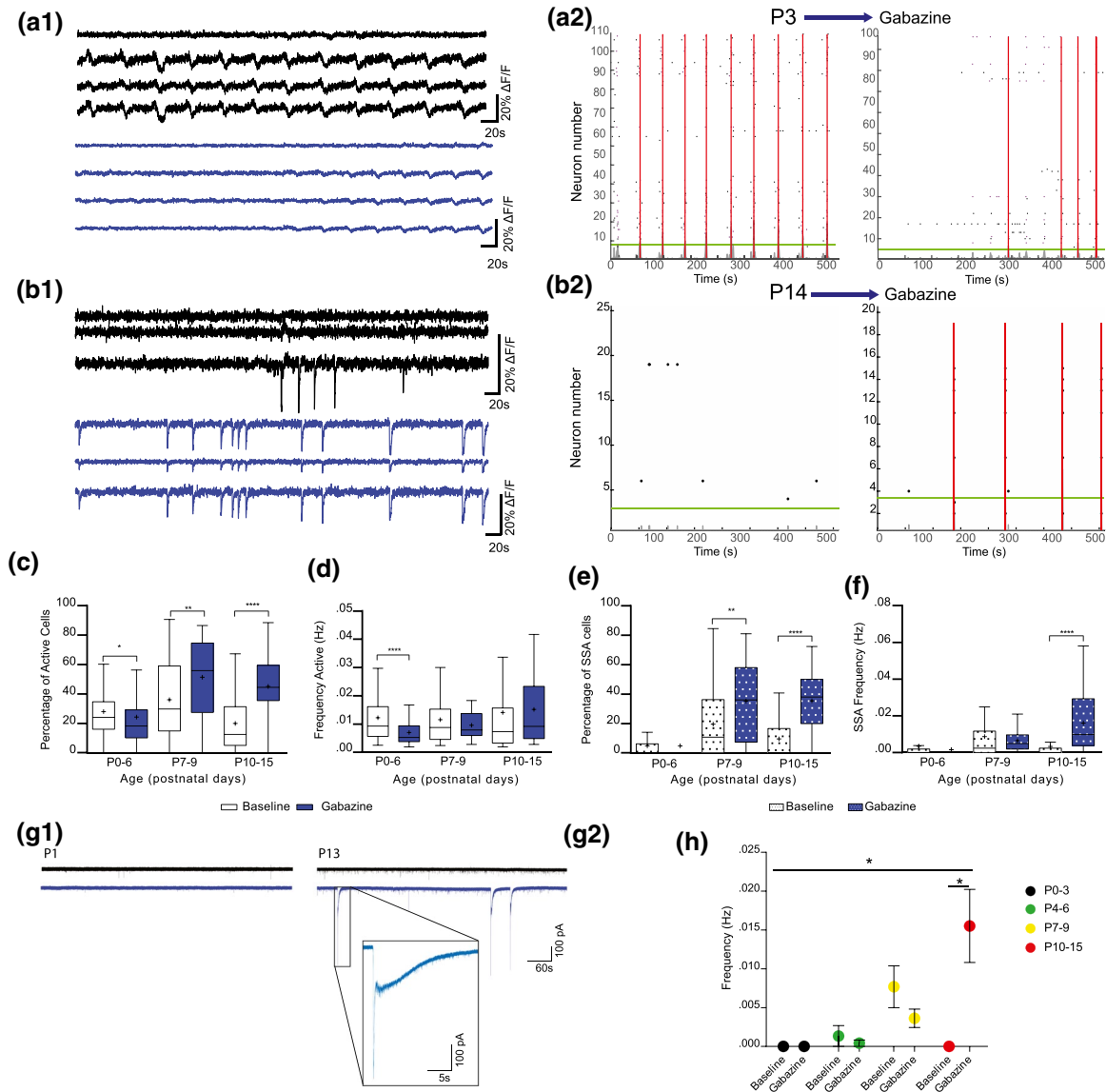
FIGURE 6 Age-dependent effects of GABAergic signaling upon SSA in mPFC. (a1) Representative calcium fluorescence traces from a P3 slice at baseline (black) and after incubation with Gabazine (blue). The first trace in each condition shows a silent cell. (a2) Raster plots from the slice where traces in A1 were extracted showing the decrease in frequency of active cells and SSA after the application of Gabazine. (b1) Representative calcium fluorescence traces from a P14 slice at baseline (black) and after incubation with Gabazine (blue). The two first traces in black denote silent cells. (b2) Raster plots from the slice where traces in B1 were extracted. Incubation with Gabazine increased the percentage of active cells, cells in SSA, and the increase in SSA frequency. (c) Gabazine significantly reduced the percentage of active cells in the P0–6 group (Mann–Whitney U = 2,509, p = .0344) while significantly increasing it at P7–9 (Mann–Whitney U = 1,204, p = .0022) and prominently at P10–15 (Mann–Whitney U = 437, p < .0001). (d) At the level of frequency of active cells incubation with Gabazine led to a significant decrease in the P0–6 group (Mann–Whitney U = 1886, p = .0001), however, it did not show any significant effect on older age groups. (e) Gabazine presence did not significantly influence the percentage of SSA cells in P0–6. At P7–9, inhibiting GABA$_A$ receptors increased the percentage of SSA cells significantly (Mann–Whitney U = 1,201, p = .0016) with the same effect being even more evidently seen in the P10–15 group (Mann–Whitney U = 366, p < .0001). (f) SSA frequency was not significantly affected by Gabazine in the first two age groups, while the P10–15 group showed a significant increase by gabazine (Mann–Whitney U = 111, p < .0001). (g1) Representative recordings of sEPSCs from a neonatal (P1) layer 5 mPFC PC, both baseline (black) and Gabazine (blue) showed low levels of activity and no burst discharges. (g2) Representative recordings of sEPSCs from a P13 layer 5 mPFC PC where gabazine (blue) presented multiple burst discharges. The insert shows an expanded view of the transient in (h) to demonstrate the typical shape of the burst found, where one large depolarization (>2000 pA) if followed by a prolonged repolarization phase with multiple action potentials. (h) Total number of burst discharges detected either at baseline level of after the incubation with gabazine. A significant effect was found over age groups (F (3, 94) = 7.788, p = .0001) and the presence of Gabazine also had an effect (two-way ANOVA F (1, 94) = 11.64, p = .001) especially at the end of the second postnatal week (Sidak's multiple comparisons test- Baseline: P10–15 vs. Gabazine: P10–15 ****). Mean is represented by + symbol. Median represented together with minimum and maximum values. * p < .05, ** p < .01, *** p < .001, **** p < .0001. *For calcium imaging (c–f) n = number of slices: P0–6 baseline n = 160, Gabazine = 40; P7–9 baseline n = 112, Gabazine = 33; P10–15 baseline n = 92, Gabazine = 23. For patch-clamp (i) n = number of cells: P1–3 baseline n = 6; P4–6 baseline n = 21; P7–9 baseline n = 22; P10–15 baseline n = 8* [Color figure can be viewed at wileyonlinelibrary.com]

Blockade of GABA$_A$ receptors with Gabazine significantly reduced the percentage of spontaneously active cells in the P0–6 group (Figure 6c median baseline = 24%, Gabazine = 18%, Mann–Whitney U = 2,509, p = .0344) while increasing this percentage in the older age groups (P7–9 median baseline = 30%, Gabazine = 56%, Mann–Whitney U = 1,204, p = .0022; P10–15 median baseline = 13%, Gabazine = 44%, Mann–Whitney U = 437, p < .0001). It also induced a significant decrease in the frequency of active cells of the P0–6 group (P0–6 median baseline = 0.009 Hz, Gabazine = 0.005 Hz, Mann–Whitney U = 1,886, p = .0001) but, did not significantly change the frequency of active cells in older age groups (Figure 6d).

Unlike spontaneous activity, Gabazine did not significantly alter the percentage of synchronous cells or SSA frequency in the P0–6 group. It should, however, be noted that this group presents low baseline levels for both these parameters (Figure 6e,f (Percentage of SSA cell P0–6 mean baseline = 5 ± 0.8% median = 0, Gabazine = 5±2% median = 0; Frequency SSA cell P0–6 median baseline = 0.0035 ± 0.0007 Hz median = 0, Gabazine = 0.0014 ± 0.0005 Hz median = 0)). However, at P7–9, blockade of GABAergic inhibition increased significantly the percentage of synchronized cells (P7–9 median baseline = 11%, Gabazine = 36%, Mann–Whitney U = 1,201, p = .0016) but without increasing SSA frequency significantly (P7–9 median baseline = 0.003 Hz, Gabazine = 0.005 Hz). During the latter half of the second postnatal week, Gabazine significantly increased both the low percentage of synchronized cells (P10–15 median baseline = 0% (mean = 10±1.7%), Gabazine = 38.10% (mean = 35.5 ± 4.4%), Mann–Whitney U = 366, p < .0001), and prominently SSA frequency (P10–15 median baseline = 0 Hz (mean = 0.0034 ± 0.0008), Gabazine = 0.01 Hz (mean = 0.016 ± 0.0034), Mann–Whitney U = 111, p < .0001).

At a single cell level, blockade of GABA$_A$ receptor-mediated inhibition involvement in a potential alteration of the level of burst discharges from layer 5 pyramidal neurons during the first two postnatal weeks was also explored (Figure 6g,h). Gabazine did not significantly affect the occurrence of burst discharges during the first postnatal week but did induce a high frequency of spontaneous discharge events from P10–15 (Figure 6h, P10–15 average baseline = 0±0 Hz vs. Gabazine 0.016 ± 0.005 bursts).

Taken together, these findings indicate that GABA$_A$ receptor-mediated inhibition significantly modulated spontaneous and synchronous mPFC network activity during the first two postnatal weeks. During the first postnatal week, GABAergic blockade significantly decreased levels of spontaneous activity, whereas in contrast, it increased both spontaneous and synchronous measures of network and single cell activity during the second postnatal week.

3.7 | Oxytocin influences early SSA but only alters spontaneous activity after P7

Oxytocin is a neuropeptide with a key role in the control of several cognitive, social, and neuroendocrine functions and best known for promoting parturition and lactation. (Meyer-Lindenberg et al., 2011; Sala et al., 2011) Maternal oxytocin was reported to directly control a first "GABA switch" during parturition (Leonzino et al., 2016; Tyzio et al., 2006). To determine whether oxytocin can acutely modulate spontaneous activity and SSA in the developing mPFC, slices were imaged before and after being exposed to 1 μM oxytocin (Figure 7a).

At the beginning of the first postnatal week oxytocin had no significant effect on either the percentage of spontaneously active cells or their frequency (Figure 7b,d). However, at P0–6 (Figure 7c,e), it negatively influenced the percentage of synchronized cells (baseline = 5±1% vs. Oxytocin = 1±1%, Mann–Whitney U = 1,008, p = .032) and the SSA frequency (baseline = 0.0035 ± 0.0007 Hz vs. Oxytocin = 0.0001 ± 0.0001 Hz, Mann–Whitney U = 971, p = .017). At later age groups, oxytocin had no effects on the percentage of synchronized cells or SSA frequency. However, oxytocin modulated the frequency of spontaneous activity in the network, causing an increase in frequency at P7–9 (baseline Mdn = 0.0087; Oxytocin Mdn = 0.016, U = 732, p = .037) but a decrease in the older age group (P10–15 baseline Mdn = 0.007; Oxytocin Mdn = 0.004, U = 334.5, p = .012).

Although SSA levels are particularly low at the start of the first postnatal week, these results give an indication that oxytocin could be used to disrupt the early but not later stages of SSA, causing desynchronization, without interfering with the general spontaneous activity of cells in the developing mPFC.

4 | DISCUSSION

The data outlines the developmental profile of spontaneous activity and the critical period of SSA in mPFC networks during the two first postnatal weeks in mice. For mPFC, the first few weeks are a period of extensive structural and functional synaptic development, similar to other neocortical regions (Feldmeyer & Radnikow, 2009; Kroon et al., 2019). During the first two postnatal weeks of mPFC development, the frequency of spontaneous network activity gradually increased, while SSA showed a distinct developmentally regulated pattern with its onset during the first week, peak activity between P8–9 and then its disappearance by P15. This was supported by electrophysiological recordings where burst discharges displayed a similar profile peaking the P7–9. Both
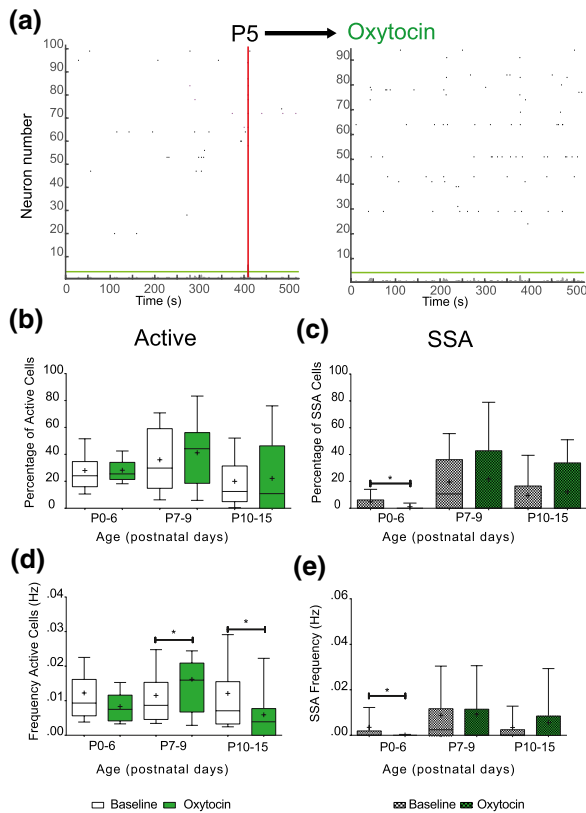
FIGURE 7 Oxytocin influences early SSA but only alters spontaneous activity after P7. (a) Representative Raster plots of the effect of Oxytocin on a P5 slice, where the low level of SSA is reduced to zero. (b) Quantification of the effect of oxytocin incubation in the several age groups test on the percentage of active cells. Oxytocin does not have any significant effect in the percentage of active cells at any age tested. (c) Oxytocin significantly reduces the percentage of SSA cells at P0–6 (Mann–Whitney U = 1,008, p = .0.032) and shows no significant effect at older age groups. (d) Incubation with oxytocin significantly increases spontaneous activity frequency at P7–9 (during the peak of activity) (Mann–Whitney—baseline Mdn = 0.0087; Oxytocin Mdn = 0.016), U = 732, p = .037) while it decreased it at P10–15 (Mann–Whitney—baseline Mdn = 0.007; Oxytocin Mdn = 0.004), U = 334.5, p = .012). (e) Oxytocin significantly reduces SSA frequency at P0–6 (Mann–Whitney U = 971, p = .017) similar to the effect it had on the percentage of SSA cells. Likewise, it did not have a significant effect on older age groups. Total number of slices per age is: P0–6 = 17, P7–9 = 19, P10–15 = 14. The + sign represents the mean and the horizontal bar the average. *p < .05; **p < .01; ***p < .001; ****p < .0001 [Color figure can be viewed at wileyonlinelibrary.com]

spontaneous and SSA were maintained on an isolated mPFC albeit to a lesser frequency and lower number of cells participating. Both were also dependent on action potential, with SSA coming to a complete block when a sodium channel blocker was present. Pharmacological blockade of gap junctions revealed a potential role of these on actually decreasing the number of cells activity and decreasing the frequency of SSA postnatally. From a mechanistic point of view SSA in

the mPFC seems to be highly dependent on ionotropic glutamatergic transmission as seen by the vast decrease (almost to a full block) of this type of activity in the presence of the blockers cocktail used at all ages measured. GABA might have small contribution to this activity on the earlier time points (P0–6) but starts assuming an inhibitory role from the end of the first postnatal week onward. Probably being the case of the extinction of the activity toward the end of its critical period. This effect is similarly seen in burst discharges in the presence of Gabazine.

On the contrary, spontaneous activity seems to be only slightly dependent on a potential excitatory role of GABA early on, with no involvement of glutamate. This suggests the involvement of a third kind of mechanism or neurotransmitter as for example acetylcholine (which was not feasible to be tested with the same protocol due to the high choline chloride concentration used during slice preparation). From the end of the first week ionotropic glutamatergic transmission has a significant positive contribution and GABA assumes its typical inhibitory role. However, the remaining levels of activity again suggest a third contributing element. Oxytocin was tested a potential contributor or modulator of early activity given its involvement in parturition and the GABA "switch" that occurs in the fetal brain during (Tyzio et al., 2006), however, it only showed some modulatory effects of synchronous activity in the first postnatal week.

Here, critical periods were defined as regulated time-windows during which sensory experience and/or intrinsic neuronal activity transmit information that is believed to be essential for normal development and refinement of neuronal circuits. These time-windows for synchronous spontaneous network activity in neocortical neurons have been investigated from late prenatal stages through to the second postnatal week in rodent brain. Comparisons between critical periods for different regions have limitations due to differences in slice/recording methodology and inexact description of the neocortical region, particularly in prenatal/early postnatal stages (see Supporting Information Table S1 for overview). For example, in somatosensory cortex in vitro, SSA (identified as "early cortical network oscillations") peaks just after birth (P0–P3) and is no longer present by P6–P8 (Allene et al., 2008) while in vivo, barrel cortex was synchronously active from its onset at P4 until P14 where it was sparsely detected (Golshani et al., 2009) In addition, an immature form of SSA has been has been reported in aged organotypic neocortical cultures of prenatal extraction (Chiappalone et al., 2007). In our study, the earliest age point measured was P0, so while we cannot rule out the presence of SSA before this time point in mPFC, it seems to be unlikely since the level of spontaneous activity at P0 was sparse and at its lowest relative to all later time points, and there was no synchronous activity present. Taking all current data together, however, there seem to be no evidence for synchronous

network activity occurring at significantly later time points in mPFC than in other neocortical regions, and thereby no support for a later critical period in rodent mPFC based on these measures.

From a mechanistic point of view, SSA in mPFC is largely driven by ionotropic glutamatergic transmission as indicated by the complete blockade of synchronous activity by ionotropic glutamatergic antagonists at all ages tested. A similar major contribution of ionotropic glutamatergic transmission to SSA has been observed in other cortical and hippocampal areas (Bolea et al., 1999; Canepari et al., 2000; Seki et al., 2012). In these regions, synaptic AMPA receptors provide the depolarization needed to remove the Mg^{2+} block, permitting the participation of NMDA receptors in the creation of synchronous activity. Although not tested in this study, a separate block of the receptors could elucidate any potentially different participation in mPFC during this time period. In contrast to the strong glutamatergic-dependence of SSA, spontaneous activity during this critical period was only partially mediated via ionotropic glutamatergic signaling. Indeed, regarding spontaneous activity in general, there were no significant effects of glutamatergic blockade during the first postnatal week, with only a significant decrease in the number of active cells from P7 onward—presumably reflecting a maturation of excitatory synaptic transmission from postnatal week 1 to 2 during early mPFC development (Kroon et al., 2019).

Unlike some forms of synchronous network activity (referred to as "giant depolarising potentials") in the immature hippocampus (Garaschuk et al., 2000; McCabe et al., 2006), SSA in the developing mPFC does not depend on excitatory GABAergic neurotransmission at its peak level. This was shown by the lack of a negative effect of the $GABA_A$ receptor-mediated antagonist, Gabazine, on both the percentage of cells participating in synchronous events and on the SSA frequency itself. Rather, blocking $GABA_A$ receptor-mediated signaling at the peak of SSA (P7–9) led to a higher percentage of synchronized cells without affecting SSA frequency, suggesting an inhibitory influence already upon network synchrony at this time point. By the end of the second postnatal week (P10–15), this negative effect upon network synchrony persisted as removal of $GABA_A$ receptor-mediated signaling restored both SSA frequency and the percentage of synchronous cells to values close to those previously observed at peak SSA levels at P7–9. These findings are supported also by the disinhibition seen in single cell recordings from layer 5 mPFC pyramidal neurons, whereby at P10–15 application of Gabazine significantly increased the frequency of burst firing discharges. These results indicate that an emergence of ionotropic GABAergic inhibition could be responsible as a mechanism for the suppression of SSA in developing mPFC networks and a major contributory factor to the closure of this critical period for synchrony. This pattern of inhibitory

maturation at the cellular level is similar to that reported in the CA3 area of the hippocampus where a period of enhanced excitability is terminated with the developmental switch in GABA-mediated function from an excitatory to an inhibitory profile (Khazipov et al., 2004). Supporting such a changing developmental profile in mPFC from initial GABAergic excitation, a small but significant decrease in spontaneous activity from P0–6 via Gabazine can be observed, although the decreases in SSA during this first postnatal week were nonsignificant, probably due to the very low level of SSA observed in only a subset of slices. It should be noted that the timing of the change of GABA from excitatory to inhibitory action, termed the GABA "switch," differs between the hippocampus and neocortex. In rodent hippocampal slices after P5, GABA exerts an excitatory action (Valeeva et al., 2013) while the somatosensory cortex shows mature levels for the reverse potential of chloride (an indicator of what action GABA will have via $GABA_A$ receptor activation) at the later age of P8–9 (He et al., 2014).

It is only possible to speculate how our findings on network development and SSAs in mPFC brain slices translates to in vivo developing mPFC. Even though there are reports of this kind of activity in vivo the use of anesthetics is a big liming factor to further evaluate it mechanistically as well as the use of genetic models as they will likely affect developmental processes. In adult mice high isoflurane doses have been shown to induce synchrony in local neuronal networks in a dose-dependent manner (Goltstein et al., 2015; Wang et al., 2020). This is thought to be by increasing activity of $GABA_A$ receptors and potassium channels. One recurring theme is also that anesthetics acting on the GABAergic system are likely to exert their effects differently on local cortical circuits, given the differences in types of neurons present and their repertoire of receptors. Adding to this the repertoire of GABAergic receptors changes during development (Wu & Sun, 2015) making it even harder to compare in vivo results over several ages when anesthetics are present. Likewise, we can only speculate whether SSA plays a role in the maturation of the network and the neuronal expression of chloride transporters NKCC1 and KCC2 that contribute toward the switch in GABA's actions (Rivera et al., 1999; Schulte et al., 2018). However, regardless, the data here presented indicate a switch in mechanism of GABAergic action that occurs at the start of the second postnatal week in rodent cortex, in agreement with that reported in the neocortex (Luhmann & Prince, 1991; Owens et al., 1996).

SSA in mPFC networks was abolished by the acute application of TTX, indicating that it is mediated by action potential-dependent activity in the slice. Electrophysiological recordings from pyramidal neurons confirmed the presence of AP burst discharges at similar frequencies to those of SSA measured using calcium-dependent indicators at peak network activity ages (see Supporting Information Figure

S1). These burst discharges were comprised of a large de-polarizing event followed by a slow-repolarization wave containing several action potentials. These events lasted on average 3 s (2.8 ± 0.8 s) similar to reports from other neocortical areas (McCabe et al., 2006) but longer than for example, events in the developing hippocampus (Ben-Ari et al., 1989; Garaschuk et al., 1998). While network synchrony in the rodent neocortex is largely mediated via local synaptic transmission, the synchronous waves of activity are reported to be initiated by extrinsic pacemakers located in regions including the piriform or entorhinal cortices, septal nuclei, hippocampus, or the contralateral cortical area (Barger et al., 2016; Easton et al., 2014; Garaschuk et al., 2000; Lischalk et al., 2009). For mPFC, the reduction of spontaneous activity and SSA seen in the minislice preparation points toward a partial dependency on other brain areas to contribute or even generate spontaneous and synchronous activity. Several connections to and from the mPFC (Riga et al., 2014) especially the hippocampal-prefrontal connections (Jin & Maren, 2015) can generate oscillations by phase-locking the neuronal firing via direct axonal pathways at an immature developmental stage (Brockmann et al., 2011). One of the limitations of in vitro experiments is the ablation of several connections between brain areas while slicing the area of interest. In addition, the manipulation used was a crude lesion approach with the potential to cause localized physical damage. However, given the continuation of SSA in a subset of isolated mPFC preparations and coupled with the persistence of neuronal firing in a small population of cells following TTX application in intact slices, it could be possible the existence of some pacemaker-like activity within the mPFC network.

In the developing rodent retina, the earliest network activity is mediated by gap junctions prior to synaptic transmission (Blankenship & Feller, 2010).Gap junctions mediate some of the earliest forms of activity measured including synchronized Ca^{2+} oscillations in small groups of neurons and precursor cells (Catsicas et al., 1998; Owens & Kriegstein, 1998). They also partially mediate synchronous plateau assemblies (SPAs) in the hippocampus of newborn mice (P0–3) (Allene et al., 2008). Similarly, the immature cerebral cortex of mice is strongly synchronized within a cortical column by gap junctions (Dupont et al., 2006). However, results in the mPFC show contradictory data, with the inhibition of gap junctions leading to an increase in the percentage of cells being spontaneously and synchronously active, and increasing the SSA frequency in slices from P0–3 animals. It must though be noted that spontaneous activity levels and SSA occurrence in mPFC was very low during the first few postnatal days tested. One hypothesis to explain the results is a disruption of inhibitory interneuron coupling leading to disinhibition of the network. While gap junction-coupled inhibitory interneurons are

extensively connected in the mature neocortex (reviewed in (Galarreta & Hestrin, 2001)) and the presence of functional GABAergic synapses at early postnatal stages has been reported (Le Magueresse & Monyer, 2013), no study has shown this to exert an inhibitory control over network activity. Furthermore, blockade of GABAergic neurotransmission in the developing mPFC networks does not support the role of GABA as having an inhibitory effect at the start of the first postnatal week but rather a small excitatory effect, since blocking phasic and tonic $GABA_A$ receptor-mediated transmission decreased network activity. One caveat of using gap junction blockers is that most of the currently available drugs tend to have low potency and effectiveness, poor selectivity, and have significant off-target effects on a wide range of non-connexin ion channels, receptors, and enzymes.(Chepkova et al., 2008; Vessey et al., 2004) Nonetheless, the results obtained with CBX point toward a small effect related to its ability to reduce connexin channel conductances (Davidson & Baumgarten, 1988) since GZA, which does not affect connexins, did not have any effect on the parameters evaluated when compared to baseline levels.

Oxytocin has a well-established role in both parturition (Arrowsmith & Wray, 2014) and lactation (Crowley, 2015) with perturbed oxytocin signaling linked to several neuropsychiatric disorders (reviewed in Cochran et al., 2013). In the developing rodent hippocampus, responses to oxytocin are derived from its effects upon GABAergic signaling (Leonzino et al., 2016; Tyzio et al., 2006) or via inhibition of glutamatergic signaling (Ripamonti et al., 2017). In mPFC, we did not observe consistent effects of acute oxytocin application upon spontaneous activity or synchrony across the first two postnatal weeks. Rather, oxytocin abolished the low level of SSA during the first postnatal week and altered the frequency of spontaneous activity at two later age groups but not levels of synchrony. Although this may hint toward an effect of oxytocin via inhibition of glutamatergic signaling, it is difficult to draw strong conclusions. Prolonged oxytocin application or an in utero manipulation may elucidate the role of oxytocin further, particularly in the early stages of SSA onset.

Finally, perturbation of network activity during critical periods or the alteration of the timing of these periods have been hypothesized as major factors for the alteration of neuronal circuit formation and maturation (Allene & Cossart, 2010; Hanganu-Opatz, 2010). Furthermore, alteration of the timing of network synchrony during critical periods may underlie pathophysiology of certain neurodevelopmental disorders (Meredith et al., 2012) including Fragile X Syndrome (Goncalves et al., 2013) and Rett Syndrome (Contractor et al., 2015; He et al., 2017; Lu et al., 2016). The mPFC plays an important role in several cognitive and executive function processes (Miller, 2000) and is vulnerable in specific neurodevelopmental disorders (Schubert et al., 2015). Knowledge of the critical periods for network

synchrony in the neurotypically developing rodent brain and the underlying mechanisms may be important for deciphering pre-frontal cortex alterations in brain disorders and the opportunity for early pharmacological manipulations with pharmacothera-peutic potential.

CONFLICT OF INTEREST
The authors have no conflicts of interest to declare.

AUTHOR CONTRIBUTIONS
JP, HM, and RM designed the experiments and wrote the manuscript. JP and RN performed the experiments, data extraction, and analysis. All the authors revised the manuscript.

DATA AVAILABILITY STATEMENT
Data will be made available by the authors upon request.

ORCID
Johny Pires [ID] https://orcid.org/0000-0002-7484-2150
Huibert D. Mansvelder [ID] https://orcid.org/0000-0003-1365-5340
Rhiannon M. Meredith [ID] https://orcid.org/0000-0003-0228-4169

REFERENCES
Allene, C., Cattani, A., Ackman, J. B., Bonifazi, P., Aniksztejn, L., Ben-Ari, Y., & Cossart, R. (2008). Sequential generation of two distinct synapse-driven network patterns in developing neocortex. *Journal of Neuroscience*, *28*(48), 12851–12863. https://doi.org/10.1523/JNEUROSCI.3733-08.2008

Allene, C., & Cossart, R. (2010). Early NMDA receptor-driven waves of activity in the developing neocortex: Physiological or pathological network oscillations? *Journal of Physiology*, *588*(Pt 1), 83–91. https://doi.org/10.1113/jphysiol.2009.178798

Arrowsmith, S., & Wray, S. (2014). Oxytocin: Its mechanism of action and receptor signalling in the myometrium. *Journal of Neuroendocrinology*, *26*(6), 356–369. https://doi.org/10.1111/jne.12154

Bani-Yaghoub, M., Underhill, T. M., & Naus, C. C. (1999). Gap junction blockage interferes with neuronal and astroglial differentiation of mouse P19 embryonal carcinoma cells. *Developmental Genetics*, *24*(1–2), 69–81. https://doi.org/10.1002/(SICI)1520-6408(1999)24:1/2<69:AID-DVG8>3.0.CO;2-M

Barger, Z., Easton, C. R., Neuzil, K. E., & Moody, W. J. (2016). Early network activity propagates bidirectionally between hippocampus and cortex. *Developmental Neurobiology*, *76*(6), 661–672. https://doi.org/10.1002/dneu.22351

Barnett, H. M., Gjorgjieva, J., Weir, K., Comfort, C., Fairhall, A. L., & Moody, W. J. (2014). Relationship between individual neuron and network spontaneous activity in developing mouse cortex. *Journal of Neurophysiology*, *112*(12), 3033–3045. https://doi.org/10.1152/jn.00349.2014

Ben-Ari, Y., Cherubini, E., Corradetti, R., & Gaiarsa, J. L. (1989). Giant synaptic potentials in immature rat CA3 hippocampal neurones. *Journal of Physiology*, *416*, 303–325. https://doi.org/10.1113/jphysiol.1989.sp017762

Ben-Ari, Y., Khalilov, I., Kahle, K. T., & Cherubini, E. (2012). The GABA excitatory/inhibitory shift in brain maturation and neurological disorders. *Neuroscientist*, *18*(5), 467–486. https://doi.org/10.1177/1073858412438697

Blankenship, A. G., & Feller, M. B. (2010). Mechanisms underlying spontaneous patterned activity in developing neural circuits. *Nature Reviews Neuroscience*, *11*(1), 18–29. https://doi.org/10.1038/nrn2759

Bolea, S., Avignone, E., Berretta, N., Sanchez-Andres, J. V., & Cherubini, E. (1999). Glutamate controls the induction of GABA-mediated giant depolarizing potentials through AMPA receptors in neonatal rat hippocampal slices. *Journal of Neurophysiology*, *81*(5), 2095–2102. https://doi.org/10.1152/jn.1999.81.5.2095

Bonifazi, P., Goldin, M., Picardo, M. A., Jorquera, I., Cattani, A., Bianconi, G., Represa, A., Ben-Ari, Y., & Cossart, R. (2009). GABAergic hub neurons orchestrate synchrony in developing hippocampal networks. *Science*, *326*(5958), 1419–1424. https://doi.org/10.1126/science.1175509

Brockmann, M. D., Poschel, B., Cichon, N., & Hanganu-Opatz, I. L. (2011). Coupled oscillations mediate directed interactions between prefrontal cortex and hippocampus of the neonatal rat. *Neuron*, *71*(2), 332–347. https://doi.org/10.1016/j.neuron.2011.05.041

Brumback, A. C., Ellwood, I. T., Kjaerby, C., Iafrati, J., Robinson, S., Lee, A. T., Patel, T., Nagaraj, S., Davatolhagh, F., & Sohal, V. S. (2018). Identifying specific prefrontal neurons that contribute to autism-associated abnormalities in physiology and social behavior. *Molecular Psychiatry*, *23*(10), 2078–2089. https://doi.org/10.1038/mp.2017.213

Bureau, I., von Saint Paul, F., & Svoboda, K. (2006). Interdigitated paralemniscal and lemniscal pathways in the mouse barrel cortex. *PLoS Biol*, *4*(12), e382.

Canepari, M., Mammano, F., Kachalsky, S. G., Rahamimoff, R., & Cherubini, E. (2000). GABA- and glutamate-mediated network activity in the hippocampus of neonatal and juvenile rats revealed by fast calcium imaging. *Cell Calcium*, *27*(1), 25–33. https://doi.org/10.1054/ceca.1999.0086

Carter, B. C., & Bean, B. P. (2009). Sodium entry during action potentials of mammalian neurons: Incomplete inactivation and reduced metabolic efficiency in fast-spiking neurons. *Neuron*, *64*(6), 898–909. https://doi.org/10.1016/j.neuron.2009.12.011

Catsicas, M., Bonness, V., Becker, D., & Mobbs, P. (1998). Spontaneous Ca^{2+} transients and their transmission in the developing chick retina. *Current Biology*, *8*(5), 283–288. https://doi.org/10.1016/S0960-9822(98)70110-1

Chamma, I., Chevy, Q., Poncer, J. C., & Levi, S. (2012). Role of the neuronal K-Cl co-transporter KCC2 in inhibitory and excitatory neurotransmission. *Frontiers in Cellular Neuroscience*, *6*, 5. https://doi.org/10.3389/fncel.2012.00005

Chepkova, A. N., Sergeeva, O. A., & Haas, H. L. (2008). Carbenoxolone impairs LTP and blocks NMDA receptors in murine hippocampus.

Neuropharmacology, *55*(2), 139–147. https://doi.org/10.1016/j.neuropharm.2008.05.001

Chiappalone, M., Vato, A., Berdondini, L., Koudelka-Hep, M., & Martinoia, S. (2007). Network dynamics and synchronous activity in cultured cortical neurons. *International Journal of Neural Systems*, *17*(2), 87–103. https://doi.org/10.1142/S0129065707000968

Chowdhury, D., & Hell, J. W. (2018). Homeostatic synaptic scaling: Molecular regulators of synaptic AMPA-type glutamate receptors. *F1000Research*, *7*, 234–243. https://doi.org/10.12688/f1000research.13561.1

Cochran, D. M., Fallon, D., Hill, M., & Frazier, J. A. (2013). The role of oxytocin in psychiatric disorders: A review of biological and therapeutic research findings. *Harvard Review of Psychiatry*, *21*(5), 219–247. https://doi.org/10.1097/HRP.0b013e3182a75b7d

Conhaim, J., Easton, C. R., Becker, M. I., Barahimi, M., Cedarbaum, E. R., Moore, J. G., Mather, L. F., Dabagh, S., Minter, D. J., Moen, S. P., & Moody, W. J. (2011). Developmental changes in propagation patterns and transmitter dependence of waves of spontaneous activity in the mouse cerebral cortex. *Journal of Physiology*, *589*(Pt 10), 2529–2541. https://doi.org/10.1113/jphysiol.2010.202382

Connors, B. W., Benardo, L. S., & Prince, D. A. (1983). Coupling between neurons of the developing rat neocortex. *Journal of Neuroscience*, *3*(4), 773–782. https://doi.org/10.1523/JNEUROSCI.03-04-00773.1983

Contractor, A., Klyachko, V. A., & Portera-Cailliau, C. (2015). Altered neuronal and circuit excitability in fragile X syndrome. *Neuron*, *87*(4), 699–715. https://doi.org/10.1016/j.neuron.2015.06.017

Corlew, R., Bosma, M. M., & Moody, W. J. (2004). Spontaneous, synchronous electrical activity in neonatal mouse cortical neurones. *Journal of Physiology*, *560*(Pt 2), 377–390. https://doi.org/10.1113/jphysiol.2004.071621

Crowley, W. R. (2015). Neuroendocrine regulation of lactation and milk production. *Comprehensive Physiology*, *5*(1), 255–291. https://doi.org/10.1002/cphy.c140029

Davidson, J. S., & Baumgarten, I. M. (1988). Glycyrrhetinic acid derivatives: A novel class of inhibitors of gap-junctional intercellular communication. Structure-activity relationships. *Journal of Pharmacology and Experimental Therapeutics*, *246*(3), 1104–1107.

Dawitz, J., Kroon, T., Hjorth, J. J. J., & Meredith, R. M. (2011). Functional calcium imaging in developing cortical networks. *Journal of Visualized Experiments*, *56*, e3550. https://doi.org/10.3791/3550

Dupont, E., Hanganu, I. L., Kilb, W., Hirsch, S., & Luhmann, H. J. (2006). Rapid developmental switch in the mechanisms driving early cortical columnar networks. *Nature*, *439*(7072), 79–83. https://doi.org/10.1038/nature04264

Easton, C. R., Weir, K., Scott, A., Moen, S. P., Barger, Z., Folch, A., Hevner, R. F., & Moody, W. J. (2014). Genetic elimination of GABAergic neurotransmission reveals two distinct pacemakers for spontaneous waves of activity in the developing mouse cortex. *Journal of Neuroscience*, *34*(11), 3854–3863. https://doi.org/10.1523/JNEUROSCI.3811-13.2014

Feldmeyer, D., & Radnikow, G. (2009). Developmental alterations in the functional properties of excitatory neocortical synapses. *Journal of Physiology*, *587*(Pt 9), 1889–1896. https://doi.org/10.1113/jphysiol.2009.169458

Galarreta, M., & Hestrin, S. (2001). Electrical synapses between GABA-releasing interneurons. *Nature Reviews Neuroscience*, *2*(6), 425–433. https://doi.org/10.1038/35077566

Gao, W., Zhu, H., Giovanello, K. S., Smith, J. K., Shen, D., Gilmore, J. H., & Lin, W. (2009). Evidence on the emergence of the brain's default network from 2-week-old to 2-year-old healthy pediatric subjects. *Proceedings of the National Academy of Sciences of the United States of America*, *106*(16), 6790–6795. https://doi.org/10.1073/pnas.0811221106

Garaschuk, O., Hanse, E., & Konnerth, A. (1998). Developmental profile and synaptic origin of early network oscillations in the CA1 region of rat neonatal hippocampus. *Journal of Physiology*, *507*(Pt 1), 219–236. https://doi.org/10.1111/j.1469-7793.1998.219bu.x

Garaschuk, O., Linn, J., Eilers, J., & Konnerth, A. (2000). Large-scale oscillatory calcium waves in the immature cortex. *Nature Neuroscience*, *3*(5), 452–459. https://doi.org/10.1038/74823

Gervain, J., Macagno, F., Cogoi, S., Pena, M., & Mehler, J. (2008). The neonate brain detects speech structure. *Proceedings of the National Academy of Sciences of the United States of America*, *105*(37), 14222–14227. https://doi.org/10.1073/pnas.0806530105

Gilbert, S. J., Bird, G., Brindley, R., Frith, C. D., & Burgess, P. W. (2008). Atypical recruitment of medial prefrontal cortex in autism spectrum disorders: An fMRI study of two executive function tasks. *Neuropsychologia*, *46*(9), 2281–2291. https://doi.org/10.1016/j.neuropsychologia.2008.03.025

Golshani, P., Goncalves, J. T., Khoshkhoo, S., Mostany, R., Smirnakis, S., & Portera-Cailliau, C. (2009). Internally mediated developmental desynchronization of neocortical network activity. *Journal of Neuroscience*, *29*(35), 10890–10899. https://doi.org/10.1523/JNEUROSCI.2012-09.2009

Goltstein, P. M., Montijn, J. S., & Pennartz, C. M. (2015). Effects of isoflurane anesthesia on ensemble patterns of Ca2+ activity in mouse v1: Reduced direction selectivity independent of increased correlations in cellular activity. *PLoS ONE*, *10*(2), e0118277. https://doi.org/10.1371/journal.pone.0118277

Goncalves, J. T., Anstey, J. E., Golshani, P., & Portera-Cailliau, C. (2013). Circuit level defects in the developing neocortex of fragile X mice. *Nature Neuroscience*, *16*(7), 903–909. https://doi.org/10.1038/nn.3415

Grossmann, T., & Johnson, M. H. (2010). Selective prefrontal cortex responses to joint attention in early infancy. *Biology Letters*, *6*(4), 540–543. https://doi.org/10.1098/rsbl.2009.1069

Hanganu-Opatz, I. L. (2010). Between molecules and experience: Role of early patterns of coordinated activity for the development of cortical maps and sensory abilities. *Brain Research Reviews*, *64*(1), 160–176. https://doi.org/10.1016/j.brainresrev.2010.03.005

He, C. X., Cantu, D. A., Mantri, S. S., Zeiger, W. A., Goel, A., & Portera-Cailliau, C. (2017). Tactile defensiveness and impaired adaptation of neuronal activity in the Fmr1 knock-out mouse model of autism. *Journal of Neuroscience*, *37*(27), 6475–6487. https://doi.org/10.1523/JNEUROSCI.0651-17.2017

He, Q., Nomura, T., Xu, J., & Contractor, A. (2014). The developmental switch in GABA polarity is delayed in fragile X mice. *Journal of Neuroscience*, *34*(2), 446–450. https://doi.org/10.1523/JNEUROSCI.4447-13.2014

Hestrin, S. (1992). Developmental regulation of NMDA receptor-mediated synaptic currents at a central synapse. *Nature*, *357*(6380), 686–689. https://doi.org/10.1038/357686a0

Hjorth, J. J. J., Dawitz, J., Kroon, T., Pires, J., Dassen, V. J., Berkhout, J. A., Emperador Melero, J., Nadadhur, A. G., Alevra, M., Toonen, R. F., Heine, V. M., Mansvelder, H. D., & Meredith, R. M. (2016). Detection of silent cells, synchronization and modulatory activity in

developing cellular networks. *Developmental Neurobiology*, *76*(4), 357–374. https://doi.org/10.1002/dneu.22319

Jin, J., & Maren, S. (2015). Prefrontal-hippocampal interactions in memory and emotion. *Frontiers in Systems Neuroscience*, *9*, 170. https://doi.org/10.3389/fnsys.2015.00170

Kandler, K., & Katz, L. C. (1998). Coordination of neuronal activity in developing visual cortex by gap junction-mediated biochemical communication. *Journal of Neuroscience*, *18*(4), 1419–1427. https://doi.org/10.1523/JNEUROSCI.18-04-01419.1998

Khazipov, R., Khalilov, I., Tyzio, R., Morozova, E., Ben-Ari, Y., & Holmes, G. L. (2004). Developmental changes in GABAergic actions and seizure susceptibility in the rat hippocampus. *European Journal of Neuroscience*, *19*(3), 590–600. https://doi.org/10.1111/j.0953-816X.2003.03152.x

Khazipov, R., & Luhmann, H. J. (2006). Early patterns of electrical activity in the developing cerebral cortex of humans and rodents. *Trends in Neurosciences*, *29*(7), 414–418. https://doi.org/10.1016/j.tins.2006.05.007

Kroon, T., van Hugte, E., van Linge, L., Mansvelder, H. D., & Meredith, R. M. (2019). Early postnatal development of pyramidal neurons across layers of the mouse medial prefrontal cortex. *Scientific Reports*, *9*(1), 5037–5053. https://doi.org/10.1038/s41598-019-41661-9

Lauri, S. E., Lamsa, K., Pavlov, I., Riekki, R., Johnson, B. E., Molnar, E., Rauvala, H., & Taira, T. (2003). Activity blockade increases the number of functional synapses in the hippocampus of newborn rats. *Molecular and Cellular Neurosciences*, *22*(1), 107–117. https://doi.org/10.1016/s1044-7431(02)00012-x

Le Magueresse, C., & Monyer, H. (2013). GABAergic interneurons shape the functional maturation of the cortex. *Neuron*, *77*(3), 388–405. https://doi.org/10.1016/j.neuron.2013.01.011

Lee, A. T., Gee, S. M., Vogt, D., Patel, T., Rubenstein, J. L., & Sohal, V. S. (2014). Pyramidal neurons in prefrontal cortex receive subtype-specific forms of excitation and inhibition. *Neuron*, *81*(1), 61–68. https://doi.org/10.1016/j.neuron.2013.10.031

Leonzino, M., Busnelli, M., Antonucci, F., Verderio, C., Mazzanti, M., & Chini, B. (2016). The timing of the excitatory-to-inhibitory GABA switch is regulated by the oxytocin receptor via KCC2. *Cell Reports*, *15*(1), 96–103. https://doi.org/10.1016/j.celrep.2016.03.013

Lischalk, J. W., Easton, C. R., & Moody, W. J. (2009). Bilaterally propagating waves of spontaneous activity arising from discrete pacemakers in the neonatal mouse cerebral cortex. *Developmental Neurobiology*, *69*(7), 407–414. https://doi.org/10.1002/dneu.20708

Lu, H., Ash, R. T., He, L., Kee, S. E., Wang, W., Yu, D., Hao, S., Meng, X., Ure, K., Ito-Ishida, A., Tang, B., Sun, Y., Ji, D., Tang, J., Arenkiel, B. R., Smirnakis, S. M., & Zoghbi, H. Y.. (2016). Loss and gain of MeCP2 cause similar hippocampal circuit dysfunction that is rescued by deep brain stimulation in a Rett syndrome mouse model. *Neuron*, *91*(4), 739–747. https://doi.org/10.1016/j.neuron.2016.07.018

Luczak, A., & MacLean, J. (2012). Default activity patterns at the neocortical microcircuit level. *Frontiers in Integrative Neuroscience*, *6*(30), 1–6. https://doi.org/10.3389/fnint.2012.00030

Luhmann, H. J., & Khazipov, R. (2018). Neuronal activity patterns in the developing barrel cortex. *Neuroscience*, *368*, 256–267. https://doi.org/10.1016/j.neuroscience.2017.05.025

Luhmann, H. J., & Prince, D. A. (1991). Postnatal maturation of the GABAergic system in rat neocortex. *Journal of Neurophysiology*, *65*(2), 247–263. https://doi.org/10.1152/jn.1991.65.2.247

Luhmann, H. J., Sinning, A., Yang, J. W., Reyes-Puerta, V., Stuttgen, M. C., Kirischuk, S., & Kilb, W. (2016). Spontaneous neuronal activity in developing neocortical networks: From single cells to large-scale interactions. *Frontiers in Neural Circuits*, *10*, 40. https://doi.org/10.3389/fncir.2016.00040

McCabe, A. K., Chisholm, S. L., Picken-Bahrey, H. L., & Moody, W. J. (2006). The self-regulating nature of spontaneous synchronized activity in developing mouse cortical neurones. *Journal of Physiology*, *577*(Pt 1), 155–167. https://doi.org/10.1113/jphysiol.2006.117523

McCabe, A. K., Easton, C. R., Lischalk, J. W., & Moody, W. J. (2007). Roles of glutamate and GABA receptors in setting the developmental timing of spontaneous synchronized activity in the developing mouse cortex. *Developmental Neurobiology*, *67*(12), 1574–1588. https://doi.org/10.1002/dneu.20533

Meredith, R. M., Dawitz, J., & Kramvis, I. (2012). Sensitive time-windows for susceptibility in neurodevelopmental disorders. *Trends in Neurosciences*, *35*(6), 335–344. https://doi.org/10.1016/j.tins.2012.03.005

Meyer-Lindenberg, A., Domes, G., Kirsch, P., & Heinrichs, M. (2011). Oxytocin and vasopressin in the human brain: Social neuropeptides for translational medicine. *Nature Reviews Neuroscience*, *12*(9), 524–538. https://doi.org/10.1038/nrn3044

Miller, E. K. (2000). The prefrontal cortex and cognitive control. *Nature Reviews Neuroscience*, *1*(1), 59–65. https://doi.org/10.1038/35036228

Moody, W. J., & Bosma, M. M. (2005). Ion channel development, spontaneous activity, and activity-dependent development in nerve and muscle cells. *Physiological Reviews*, *85*(3), 883–941. https://doi.org/10.1152/physrev.00017.2004

Owens, D. F., Boyce, L. H., Davis, M. B., & Kriegstein, A. R. (1996). Excitatory GABA responses in embryonic and neonatal cortical slices demonstrated by gramicidin perforated-patch recordings and calcium imaging. *Journal of Neuroscience*, *16*(20), 6414–6423. https://doi.org/10.1523/JNEUROSCI.16-20-06414.1996

Owens, D. F., & Kriegstein, A. R. (1998). Patterns of intracellular calcium fluctuation in precursor cells of the neocortical ventricular zone. *Journal of Neuroscience*, *18*(14), 5374–5388. https://doi.org/10.1523/JNEUROSCI.18-14-05374.1998

Picardo, M. A., Guigue, P., Bonifazi, P., Batista-Brito, R., Allene, C., Ribas, A., Fishell, G., Baude, A., & Cossart, R. (2011). Pioneer GABA cells comprise a subpopulation of hub neurons in the developing hippocampus. *Neuron*, *71*(4), 695–709. https://doi.org/10.1016/j.neuron.2011.06.018

Picken Bahrey, H. L., & Moody, W. J. (2003). Early development of voltage-gated ion currents and firing properties in neurons of the mouse cerebral cortex. *Journal of Neurophysiology*, *89*(4), 1761–1773. https://doi.org/10.1152/jn.00972.2002

Pirone, A., Alexander, J. M., Koenig, J. B., Cook-Snyder, D. R., Palnati, M., Wickham, R. J., Eden, L., Shrestha, N., Reijmers, L., Biederer, T., Miczek, K. A., Dulla, C. G., & Jacob, M. H. (2018). Social stimulus causes aberrant activation of the medial prefrontal cortex in a mouse model with autism-like behaviors. *Frontiers in Synaptic Neuroscience*, *10*, 35. https://doi.org/10.3389/fnsyn.2018.00035

Riga, D., Matos, M. R., Glas, A., Smit, A. B., Spijker, S., & Van den Oever, M. C. (2014). Optogenetic dissection of medial prefrontal cortex circuitry. *Frontiers in Systems Neuroscience*, *8*, 230. https://doi.org/10.3389/fnsys.2014.00230

Ripamonti, S., Ambrozkiewicz, M. C., Guzzi, F., Gravati, M., Biella, G., Bormuth, I., Hammer, M., Tuffy, L. P., Sigler, A., Kawabe, H., Nishimori, K., Toselli, M., Brose, N., Parenti, M., & Rhee,

J. S. (2017). Transient oxytocin signaling primes the development and function of excitatory hippocampal neurons. *eLife*, *6*, e22466–e22497. https://doi.org/10.7554/eLife.22466

Rivera, C., Voipio, J., Payne, J. A., Ruusuvuori, E., Lahtinen, H., Lamsa, K., Pirvola, U., Saarma, M., & Kaila, K. (1999). The K+/Cl- co-transporter KCC2 renders GABA hyperpolarizing during neuronal maturation. *Nature*, *397*(6716), 251–255. https://doi.org/10.1038/16697

Sala, M., Braida, D., Lentini, D., Busnelli, M., Bulgheroni, E., Capurro, V., Finardi, A., Donzelli, A., Pattini, L., Rubino, T., Parolaro, D., Nishimori, K., Parenti, M., & Chini, B. (2011). Pharmacologic rescue of impaired cognitive flexibility, social deficits, increased aggression, and seizure susceptibility in oxytocin receptor null mice: A neurobehavioral model of autism. *Biological Psychiatry*, *69*(9), 875–882. https://doi.org/10.1016/j.biopsych.2010.12.022

Schubert, D., Martens, G. J., & Kolk, S. M. (2015). Molecular underpinnings of prefrontal cortex development in rodents provide insights into the etiology of neurodevelopmental disorders. *Molecular Psychiatry*, *20*(7), 795–809. https://doi.org/10.1038/mp.2014.147

Schulte, J. T., Wierenga, C. J., & Bruining, H. (2018). Chloride transporters and GABA polarity in developmental, neurological and psychiatric conditions. *Neuroscience and Biobehavioral Reviews*, *90*, 260–271. https://doi.org/10.1016/j.neubiorev.2018.05.001

Seki, M., Kobayashi, C., Takahashi, N., Matsuki, N., & Ikegaya, Y. (2012). Synchronized spike waves in immature dentate gyrus networks. *European Journal of Neuroscience*, *35*(5), 673–681. https://doi.org/10.1111/j.1460-9568.2012.07995.x

Siegel, F., Heimel, J. A., Peters, J., & Lohmann, C. (2012). Peripheral and central inputs shape network dynamics in the developing visual cortex in vivo. *Current Biology*, *22*(3), 253–258. https://doi.org/10.1016/j.cub.2011.12.026

Song, C., & Moyer, J. R., Jr. (2018). Layer- and subregion-specific differences in the neurophysiological properties of rat medial prefrontal cortex pyramidal neurons. *Journal of Neurophysiology*, *119*(1), 177–191. https://doi.org/10.1152/jn.00146.2017

Stacy, R. C., Demas, J., Burgess, R. W., Sanes, J. R., & Wong, R. O. (2005). Disruption and recovery of patterned retinal activity in the absence of acetylcholine. *Journal of Neuroscience*, *25*(41), 9347–9357. https://doi.org/10.1523/JNEUROSCI.1800-05.2005

Sutor, B., & Hagerty, T. (2005). Involvement of gap junctions in the development of the neocortex. *Biochimica et Biophysica Acta*, *1719*(1–2), 59–68. https://doi.org/10.1016/j.bbamem.2005.09.005

Thomas, M. S. C., & Johnson, M. H. (2008). New advances in understanding sensitive periods in brain development. *Current Directions in Psychological Science*, *17*(1), 1–5. https://doi.org/10.1111/j.1467-8721.2008.00537.x

Turrigiano, G. G., & Nelson, S. B. (2004). Homeostatic plasticity in the developing nervous system. *Nature Reviews Neuroscience*, *5*(2), 97–107. https://doi.org/10.1038/nrn1327

Tyzio, R., Cossart, R., Khalilov, I., Minlebaev, M., Hubner, C. A., Represa, A., Ben-Ari, Y., & Khazipov, R. (2006). Maternal oxytocin triggers a transient inhibitory switch in GABA signaling in the fetal brain during delivery. *Science*, *314*(5806), 1788–1792. https://doi.org/10.1126/science.1133212

Valeeva, G., Valiullina, F., & Khazipov, R. (2013). Excitatory actions of GABA in the intact neonatal rodent hippocampus in vitro. *Frontiers in Cellular Neuroscience*, *7*, 20. https://doi.org/10.3389/fncel.2013.00020

Vessey, J. P., Lalonde, M. R., Mizan, H. A., Welch, N. C., Kelly, M. E., & Barnes, S. (2004). Carbenoxolone inhibition of voltage-gated Ca channels and synaptic transmission in the retina. *Journal of Neurophysiology*, *92*(2), 1252–1256. https://doi.org/10.1152/jn.00148.2004

Wang, H. Y., Eguchi, K., Yamashita, T., & Takahashi, T. (2020). Frequency-dependent block of excitatory neurotransmission by isoflurane via dual presynaptic mechanisms. *Journal of Neuroscience*, *40*(21), 4103–4115. https://doi.org/10.1523/JNEUROSCI.2946-19.2020

Wu, C., & Sun, D. (2015). GABA receptors in brain development, function, and injury. *Metabolic Brain Disease*, *30*(2), 367–379. https://doi.org/10.1007/s11011-014-9560-1

Yang, J. W., Hanganu-Opatz, I. L., Sun, J. J., & Luhmann, H. J. (2009). Three patterns of oscillatory activity differentially synchronize developing neocortical networks in vivo. *Journal of Neuroscience*, *29*(28), 9011–9025. https://doi.org/10.1523/JNEUROSCI.5646-08.2009

Yuste, R., Peinado, A., & Katz, L. C. (1992). Neuronal domains in developing neocortex. *Science*, *257*(5070), 665–669.

SUPPORTING INFORMATION

Additional Supporting Information may be found online in the Supporting Information section.

How to cite this article: Pires J, Nelissen R, Mansvelder HD, Meredith RM. Spontaneous synchronous network activity in the neonatal development of mPFC in mice. *Develop Neurobiol*. 2021;81:207–225. https://doi.org/10.1002/dneu.22811